



HAL
open science

The impact of changes in sea level and East Asian monsoon on sediment transport on the Sunda Shelf since the last deglaciation

Kaikai Wu, Shengfa Liu, Xuefa Shi, Christophe Colin, Hui Zhang, Franck Bassinot, Zhifei Liu, Xisheng Fang, Serge Miska, Julius Nouet, et al.

► To cite this version:

Kaikai Wu, Shengfa Liu, Xuefa Shi, Christophe Colin, Hui Zhang, et al.. The impact of changes in sea level and East Asian monsoon on sediment transport on the Sunda Shelf since the last deglaciation. *Journal of Geophysical Research: Earth Surface*, 2023, 128 (10), pp.e2023JF007335. 10.1029/2023JF007335 . hal-04216893

HAL Id: hal-04216893

<https://hal.science/hal-04216893>

Submitted on 13 Oct 2023

HAL is a multi-disciplinary open access archive for the deposit and dissemination of scientific research documents, whether they are published or not. The documents may come from teaching and research institutions in France or abroad, or from public or private research centers.

L'archive ouverte pluridisciplinaire **HAL**, est destinée au dépôt et à la diffusion de documents scientifiques de niveau recherche, publiés ou non, émanant des établissements d'enseignement et de recherche français ou étrangers, des laboratoires publics ou privés.

JGR Earth Surface

RESEARCH ARTICLE

10.1029/2023JF007335

Key Points:

- Clay minerals and Sr-Nd isotopes identified sediment sources to the Sunda Shelf since the last deglaciation as Mekong and Thailand rivers
- Estimation of the Mekong and Thailand river inputs to the sedimentation of the Sunda Shelf and the southern South China Sea
- Sea-level rise and East Asian winter monsoon strengthening drove major sediment-source changes on the Sunda Shelf at 7.5 ka BP

Supporting Information:

Supporting Information may be found in the online version of this article.

Correspondence to:

X. Shi and C. Colin,
xfshi@fio.org.cn;
christophe.colin@universite-paris-saclay.fr

Citation:

Wu, K., Liu, S., Shi, X., Colin, C., Zhang, H., Bassinot, F., et al. (2023). The impact of changes in sea level and East Asian monsoon on sediment transport on the Sunda Shelf since the last deglaciation. *Journal of Geophysical Research: Earth Surface*, 128, e2023JF007335. <https://doi.org/10.1029/2023JF007335>

Received 28 JUL 2023

Accepted 10 SEP 2023

The Impact of Changes in Sea Level and East Asian Monsoon on Sediment Transport on the Sunda Shelf Since the Last Deglaciation

Kaikai Wu¹, Shengfa Liu^{1,2} , Xuefa Shi^{1,2} , Christophe Colin³, Hui Zhang¹, Franck Bassinot⁴ , Zhifei Liu⁵ , Xisheng Fang^{1,2} , Serge Miska³, Julius Nouet³ , Rosella Pinna-Jamme³, Arnaud Dapoigny⁴, Che Abd. Rahim Mohamed⁶, Somkiat Khokiattiwong⁷, and Narumol Kornkanitnan⁷

¹Key Laboratory of Marine Geology and Metallogeny, First Institute of Oceanography, Ministry of Natural Resources, Qingdao, China, ²Laboratory for Marine Geology, Laoshan Laboratory, Qingdao, China, ³Université Paris-Saclay, CNRS, GEOPS, Orsay, France, ⁴Laboratoire des Sciences du Climat et de l'Environnement, LSCE/IPSL, CEA-CNRS-UVSQ, Université Paris-Saclay, Gif-sur-Yvette, France, ⁵State Key Laboratory of Marine Geology, Tongji University, Shanghai, China, ⁶Faculty of Science and Technology, National University of Malaysia, Selangor, Malaysia, ⁷Department of Marine and Coastal Resources, Marine and Coastal Resources Research and Development Institute, Ministry of Natural Resources and Environment, Bangkok, Thailand

Abstract The Sunda Shelf plays a key role in the sedimentation of the southern South China Sea (SCS). However, the impact of past climate changes on sediment transfer to the Sunda Shelf and the southern SCS is still unresolved. Here, we present new data on grain size, clay mineralogy, and Sr-Nd isotopes of three marine cores, river sediments, and surface sediments of the Sunda Shelf. The results indicate that clay fractions of the central Sunda Shelf and the Gulf of Thailand derived mainly from the Mekong River and the rivers of northern Thailand since the last deglaciation. Significant changes in sediment sources are observed at 7.5 cal ka BP. From 13.3 to 7.5 cal ka BP, sediments in the Gulf of Thailand mainly originated from the rivers of northern Thailand, with contributions from the Mekong River increasing after 7.5 cal ka BP. An opposite shift is observed in the central Sunda Shelf. Such variations in the spatial distribution result from a combination of sea level and East Asian monsoon effects. After 7.5 cal ka BP, less Mekong River sediments were transported southeastwards into the southern SCS, and more sediments were gradually trapped within the delta and transported in a southwesterly direction into the Gulf of Thailand due to intense East Asian winter monsoon, which forced a strong southwestward coastal current. Our results demonstrate the important impact of East Asian winter monsoon strengthening and sea level rise in the mid-Holocene, which can change sediment sources and transport processes on the Sunda Shelf.

Plain Language Summary Sea level and monsoon are two important factors controlling sediment transfer in the tropical and subtropical continental marginal seas. However, the impact of past sea level and monsoon changes on mineralogical composition and sediment transfer to the Sunda Shelf (the largest low-latitude continental shelf) and the southern South China Sea (SCS) is unclear. This study provides new data on grain size, clay mineralogy, and Sr-Nd isotopes of sediment from marine cores, river sediments, and surface sediments of the Sunda Shelf to constrain sediment sources and climatic control on sediments deposited on the Sunda Shelf since the last deglaciation. We find that the Mekong River and the rivers of northern Thailand are two major sediment sources to the Sunda Shelf. An opposite shift of sediment sources at 7.5 cal ka BP is observed between the Gulf of Thailand and the central Sunda Shelf, which results from the transfer of the Mekong River sediments between the southern SCS and the Sunda Shelf caused by sea-level rise and East Asian winter monsoon strengthening in the mid-Holocene. Our results highlight that sea level and East Asian winter monsoons can significantly change sediment sources and transport processes on the Asian low-latitude continental shelf.

1. Introduction

The re-routing of sediments on shelves during glacial and interglacial changes of the Quaternary strongly impacted deep-sea sedimentation, particularly in the context of large shelves such as the Sunda Shelf. Such large shelves can modify the dynamic of sediment transport with the cycle of deposition and reworking of sediments during sea-level changes (Boulay et al., 2005; Colin et al., 2010; Jiwarungrueangkul, Liu, & Zhao, 2019) and weathering

of sediments during low-level stands (Boulay et al., 2007; Desiage et al., 2023; Liu et al., 2005; Wan et al., 2017). However, the impacts of past climate and oceanographic changes (e.g., monsoon and sea level changes) on sedimentary composition and sediment transfer to the Sunda Shelf and deep-sea basins of the southern South China Sea (SCS) are still not well established.

The Sunda Shelf is the largest low-latitude shelf and has received large number of sediments (>250 Mt/yr) from several rivers draining the eastern Tibetan Plateau in the North or tectonically stable regions to the West and the South (Hanebuth et al., 2003, 2011; Milliman & Syvitski, 1992). The sediment discharge of the Mekong River is high (160 Mt/yr) and the Mekong River is considered one of the dominant sediment sources to the Sunda Shelf, with significant contributions of sediments from surrounding small rivers mainly distributed offshore (>80 Mt/yr for all the small rivers of Thailand, Malay Peninsula, Sumatra, and Borneo) (Liu et al., 2016). The Sunda Shelf was exposed during glacial low sea-level stand (−120 m during the last glacial maximum-LGM (26–20 ka)) (Armstrong et al., 2019), and sediments transported by small rivers to the Gulf of Thailand were partially transported to the southern SCS deep basin by the Paleo-Chao Phraya River (Alqahtani et al., 2015). The Paleo-Chao Phraya River had an estimated drainage area of about 1,350,000 km², which was possibly the largest river system on the Sunda Shelf during the Pleistocene (Alqahtani et al., 2015). In addition, during the glacial period, sediment from the Mekong River was directly transported along the Paleo-Mekong River valley into the southern margin of the SCS (Colin et al., 2010; Jiwarungueangkul, Liu, & Zhao, 2019). Therefore, temporal and spatial distributions of sedimentation need to be studied to better constrain the role of the Sunda Shelf in the sedimentation of the southern deep-sea basin of the SCS during the late Quaternary.

Uncertainty regarding provenance is a major obstacle to extracting paleoclimatic and paleoenvironmental information from sedimentary records. Since the last deglaciation, the intensity of the East Asian winter and summer monsoons has significantly changed (Dykoski et al., 2005; Yancheva et al., 2007). Variations in monsoon rainfall intensity have been shown to modify sediment production and transport (e.g., Colin et al., 1999, 2010; Hu et al., 2012; Wan et al., 2015; Xue et al., 2010). Furthermore, changes in the relative intensity of summer and winter monsoons can also affect dominant ocean surface currents, which play a crucial role in sediment transport on the shelf. Due to the wide extent of the shelf (800 km) and its low bathymetric gradient (1:9,000 m), small changes in sea level result in large changes in the exposed shelf area (Hanebuth et al., 2003). Since the LGM, the sea level in the Sunda Shelf has increased by approximately 120 m (Hanebuth et al., 2000, 2009). The Sunda Shelf was gradually flooded, with the superimposition of several rapid sea-level rise events (Hanebuth et al., 2011). The rapid rise of sea level has caused the submergence of exposed land, and the corresponding sedimentary process, sources, and sedimentary environment will also have changed. All these processes modified the amount of sediment, the sedimentary source, and the state of chemical weathering of sediment transported to the deep-sea basin.

Clay mineral assemblages together with strontium (Sr) and neodymium (Nd) isotopic compositions of deep-sea and shelf sediments from the SCS have been demonstrated to be reliable tracers to constrain past changes in sediment sources transported to the SCS (Boulay et al., 2005, 2007; Liu et al., 2010, 2016; Sang et al., 2022; Wei et al., 2012; Wu et al., 2021), although clay mineral and Sr isotope could also be used to indicate the intensity of chemical weathering affecting drainage basins (Blum & Erel, 1995; Clift, 2016; Colin et al., 2010). Up to now, these proxies have never been used to study the evolution of the late Quaternary sediments of the Sunda Shelf.

In this study, grain size distribution, clay mineral assemblage, and Sr-Nd isotopic composition in the <63 μm and <2 μm size fractions have been analyzed on sediment samples from rivers surrounding the Sunda Shelf, surface sediments from the central Sunda Shelf off the Malay Peninsula, and sediments from three gravity cores located in the central Sunda Shelf (CJB01-64 and CJB01-75) and the middle Gulf of Thailand (BT-7) (Figure 1a). The aim has been to (a) identify the sedimentary sources of the middle Gulf of Thailand and the central Sunda Shelf since the last deglaciation (13.3 cal ka BP); (b) investigate the spatial and temporal variations in the provenance of detrital sediments of the central Sunda Shelf which could receive sediments from the Mekong River and the rivers in Thailand, the Malay Peninsula, Sumatra, and Borneo; (c) constrain the climatic factors (e.g., East Asian monsoon and sea level variations) controlling the transport of siliciclastic sediments to the Sunda Shelf and the southern SCS since the last deglaciation.

2. Regional Setting

The Sunda Shelf and surrounding river basins are mainly influenced by the East Asian monsoon and the Australian monsoon (Wang et al., 2009). The subtropical zone of the Northern Sunda Shelf (including Thailand and

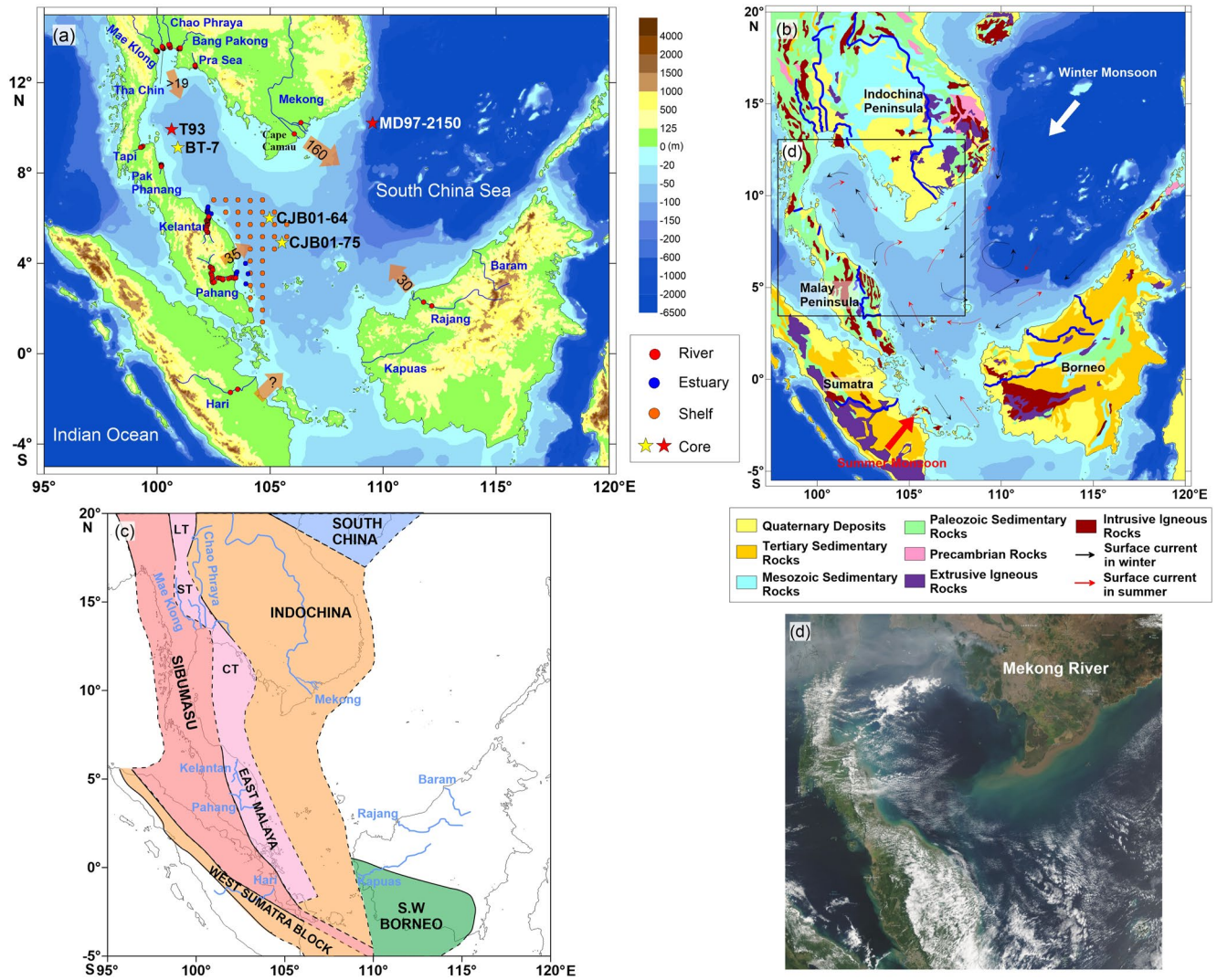


Figure 1. Sampling sites and geological setting on the Sunda Shelf. (a) Sampling sites on the Sunda Shelf and surrounding rivers. The red, blue, and orange circles represent surface sediments from the river, estuary, and Sunda Shelf, respectively. The yellow stars represent cores (BT-7, CJB01-64, and CJB01-75) of this study, and the red stars represent cores cited by Liu et al. (2004) (MD97-2150) and Chen (2020) (T93) for comparison. Orange arrows with numbers represent sediment discharge from major sources in Mt/yr revised by Liu et al. (2016). (b) Geological map and surface currents on the Sunda Shelf. The geological map was modified by Liu et al. (2016). The surface currents were revised after Fang et al. (1998), Tangang et al. (2011), and Liu et al. (2016). The rectangle indicates the location of panel (d). (c) Tectonic terranes of the Sunda Shelf and surrounding river drainages (Metcalf, 2013). LT = Lincang Terrane, ST = Sukhothai Terrane, CT = Chanthaburi Terrane. (d) MODIS image shows that Mekong River sediments are transported toward the southwest. The image is derived from <https://worldview.earthdata.nasa.gov>.

the Indochina Peninsula) is mainly under the influence of the East Asian monsoon, characterized by a seasonal reversal in wind patterns between summer and winter. The summer monsoon (from May to September) displays high temperature and precipitation with dominant southwesterly winds. In contrast, the winter monsoon (from November to January) induces low temperatures and less precipitation associated with dominant northeasterly winds (Chu & Wang, 2003). The tropical Southern Sunda Shelf (including the shelf of the eastern Malay Peninsula, Sumatra, and northern Borneo) is influenced by the East Asian-Australian monsoon systems. This region is affected by the southwesterly East Asian monsoon from September to February with high precipitation, while it is influenced by the northeasterly Australian monsoon from March to August with less precipitation (Liu et al., 2012). Additionally, it is characterized by small seasonal temperature variations throughout the year.

The surface circulation in the southern SCS is mainly controlled by seasonal monsoon wind reversal (Figure 1b; Tangang et al., 2011). In winter, the entire southern SCS is occupied by a cyclonic gyre, which reaches the northern Sunda Shelf. In summer, the reversed anticyclonic gyre occupies this region. At a latitude of approximately

11°N, the northern boundary of the anticyclonic gyre is underlined by the southeast Vietnam Offshore Current, a strong offshore-directed current (Fang et al., 1998). In the Gulf of Thailand, surface currents are mainly forced by seasonal monsoon wind reversal accompanied by anticyclonic gyre in summer (March–August) and cyclonic gyre in winter (September–November) with relatively weak currents from January to February (Wattayakorn et al., 1998).

The Mekong River had a sediment discharge of 160 Mt/yr before the dam construction in the 1990s (Milliman & Syvitski, 1992). High temperatures throughout the year and extremely abundant rainfall over high topographic relief result in strong physical erosion and the transport of huge number of sediments to the Sunda Shelf. Several smaller rivers in northern Thailand supply more than 19 Mt/year of fluvial sediments to the Gulf of Thailand (Table S1 in Supporting Information S1; Milliman & Farnsworth, 2011). The sediment discharge from the small rivers in southern Thailand is negligible due to their small drainage basins and low topographic relief. The Malay Peninsula's rivers have a sediment discharge of up to 35 Mt/yr (Liu et al., 2012). However, sediment discharge data from the rivers of Sumatra and Borneo are scarce. Based on the estimation from Milliman et al. (1999), the total sediment discharges of the rivers of northern Borneo and northeastern Sumatra are 459 and 498 Mt/yr, respectively. Nevertheless, the observed sediment loads of the Rajang River in northern Borneo, like other small mountainous rivers, were only 30 Mt/yr. Therefore, more observations are necessary to better understand the fluvial sediment discharge from this region. Tectonic terranes surrounding the Sunda Shelf include Indochina, East Malaya, Sibumasu, West Sumatra, SW Borneo, and other small blocks (Figure 1c).

3. Materials and Methods

3.1. Materials

Cores CJB01-64 (104°58'06.54"E, 5°59'53.49"N, water depth 62 m, core length 158 cm) and CJB01-75 (105°31'50.94"E, 4°54'40.52"N, water depth 80 m, core length 150 cm) were collected on the central Sunda Shelf during the China-Malaysia joint cruise aboard the "R.V. DISCOVERY" in April 2018 (Figure 1). Core BT-7 was collected in the central Gulf of Thailand (100°55.23'E, 9°6.52'N, water depth 47 m, core length 486 cm) during the China-Thailand joint cruise aboard the "M.V. SEAFDEC" in March 2018 (Figure 1; Zhang et al., 2021). The lithological descriptions of these cores are reported in Supporting Information S1.

In addition, 122 surface samples were collected throughout the central Sunda Shelf off the Malay Peninsula and from fluvial drainage basins surrounding the Sunda Shelf (Figure 1; Table 2). River samples were collected from river basins of the Indochina Peninsula, Thailand, the Malay Peninsula, Sumatra, and Borneo. These samples were collected by the China-Malaysia cooperation project in October 2016, the China-Malaysia joint cruise aboard "R.V. DISCOVERY" in September 2017, and the China-Thailand cooperation project in August 2019.

3.2. Radiocarbon Dating

Well-preserved foraminifera, gastropod shells, and plant debris were used for ^{14}C dating (Table 1). Samples were physically pretreated by sonication in deionized water to remove small carbonate particles (e.g., coccoliths) that might be trapped inside the shells. Once cleaned, the samples reacted with phosphoric acid to generate CO_2 . After graphitization, the samples were dated using an accelerator mass spectrometer (AMS) at the *Beta Analytic Laboratory* (Miami, USA). The AMS instrument was calibrated to accurately measure the ratio of ^{14}C – ^{13}C between the sample graphite and a modern reference material (NIST-4990C, Oxalic acid). The obtained analytical results were expressed as a fraction of the modern reference value, which was corrected for isotopic fractionation using $\delta^{13}\text{C}$ and radiocarbon age calculations based on the conventions outlined in Stuiver and Polach (1977). The calibrated ages suggested are according to their ± 2 sigma range (95% degree of confidence). The AMS ^{14}C dates of foraminifera were then converted to calendar years (cal yr BP, BP = 1950 Common Era or CE) using CALIB version 8.20 software, which is based on the MARINE20 (Heaton et al., 2020) and assumes an adjustment for a regional marine reservoir age of -15 ± 38 years (Southon et al., 2002). The terrestrial plant debris was calibrated to calendar years using INTCAL20.

3.3. Laser Grain-Size Analyses

Laser grain-size analyses were conducted on 305 samples from cores from the central Sunda Shelf collected at every 1 cm depth interval (157 samples from core CJB01-64 and 148 samples from core CJB01-75). Measurements of the grain-size distribution of terrigenous particles were conducted using a Malvern PANalytical

Table 1
AMS¹⁴C Dating Age Model of Cores CJB01-64 and CJB01-75

Cores	Depth (cm)	Lab no.	Material	Conventional AMS ¹⁴ C age (BP)	Calibrated age range (cal a BP, 2σ, 95% probability)	Calendar age (cal a BP)
CJB01-64	10–11	Beta- 582784	Mixed benthic foraminifera	3,560 ± 30	3,471–3,121	3,296
	30–31	Beta- 582785	Mixed benthic foraminifera	4,540 ± 30	4,788–4,388	4,588
	60–61	Beta-582786	Mixed benthic foraminifera	7,110 ± 30	7,570–7,274	7,422
	95–96	Beta-582787	Gastropod shell	9,500 ± 30	10,414–10,008	10,211
	138–139	Beta-582789	Plant debris	10,420 ± 30	12,402–12,101 (73.1%)	12,252
CJB01-75	10–11	Beta- 582794	Mixed benthic foraminifera	2,060 ± 30	1,641–1,305	1,473
	30–31	Beta-582795	Mixed benthic foraminifera	2,470 ± 30	2,147–1,774	1,961
	50–51	Beta-582796	Mixed benthic foraminifera	2,550 ± 30	2,279–1,888	2,084
	80–81	Beta-582797	Mixed benthic foraminifera	3,140 ± 30	2,973–2,633	2,803
	101–102	Beta-582798	Mixed benthic foraminifera	3,380 ± 30	3,272–2,877	3,075
	127–128	Beta-582799	Mixed benthic foraminifera	3,870 ± 30	3,866–3,484	3,675
	140–141	Beta-582800	Mixed benthic foraminifera	3,900 ± 30	3,909–3,520	3,715

Mastersizer 3000 laser grain-size analyzer hosted at the *Key Laboratory of Marine Geology and Mineralization* (Ministry of Natural Resources-MNR, China). The measurements were taken within the range of 0.01–3,500 μm. Before the analyses, bulk sediment was pre-treated to remove sea salts, biogenic carbonates, and organic matter by using deionized water, HCl (0.25 N), and hydrogen peroxide (30% v/v), respectively. The samples were ultrasonicated for 10 s to disperse them completely and then quickly introduced into the machine for measurement. The repeated measurement error was less than 3%. Mastersizer 3000 software (version 3.50) and Excel software were used to process the grain size data.

3.4. Clay Mineral X-Ray Diffraction (XRD)

The clay mineral composition of 122 surface sediment samples and 184 sediment samples from cores BT-7, CJB01-64, and CJB01-75 was analyzed using the X-ray diffraction (XRD) method on the oriented <2 μm siliciclastic fraction. The bulk sediment underwent treatment with deionized water, acetic acid (25% v/v), and hydrogen peroxide (33% v/v) to remove sea salt, carbonate, and organic matter, respectively. The <2 μm fraction of the samples was then extracted by settling based on Stokes law, and oriented thin sections of clay minerals were prepared following the analytical procedure described in detail by Liu et al. (2016). The clay minerals of cores CJB01-64 and CJB01-75 were identified by XRD using a PANalytical X'Pert powder diffractometer at the *Geosciences Paris-Saclay (GEOPS) laboratory* (PANOLY's analytical facilities at the Université Paris-Saclay, France). The analysis was conducted under CuKα radiation and a Ni filter at a current and voltage of 40 mA and 45 kV, respectively. 2θ ranged from 2.6° to 31.9°, with a step size of 0.033° and step time of 161 s. The incident beam mask width is 11.6 mm. The analysis was performed under three conditions: air-dried, ethylene glycol saturation, and heating for 2 hr at 490°C. The study involved a semi-quantitative estimation of peak areas of basal reflections for major clay groups, namely smectite (15–17 Å), illite (10 Å), and kaolinite/chlorite (7 Å), using GEOPS home-made software (JaDHe) on the ethylene glycol saturation curve. The distinction between kaolinite and chlorite was made on the basis of 3.57/3.54 Å peak areas. The clay mineral data were normalized to 100%. The sample was analyzed in replicates, and the relative error margin was ±2% (2σ).

Additionally, the clay mineral compositions of core BT-7 and all surface sediments were determined using a Rigaku D/max-2500 diffractometer at the *Key Laboratory of Marine Geology and Metallogeny* (MNR, China) following a similar analytical procedure. However, as different X-ray diffractometers may slightly affect the relative proportion of clay minerals, we then duplicated the clay mineral determination of 79 surface and core sediments obtained on the Rigaku D/max-2500 diffractometer and on the PANalytical X'Pert powder diffractometer following the exact same analytical procedure used for cores BT-7, CJB01-64, and CJB01-75. Small corrections were then applied according to the linear correlations obtained from the same clay mineral between the two X-ray diffractometers. Such corrections permit us to compare our new set of results with clay mineral data sets obtained previously for the southern SCS (Liu et al., 2016).

3.5. Analyses of Nd and Sr Isotopic Compositions

Nd and Sr isotopic compositions were analyzed on the <63 and <2 μm siliciclastic fractions of 11 samples from rivers surrounding the Sunda Shelf, 32 samples from core CJB01-64, and 30 samples from core CJB01-75. Since the <63 μm fraction can be transported by ocean currents and clay minerals are mainly present in <2 μm fraction, these two fractions are chosen to minimize the grain size effect on isotopic results and compare them with clay mineral results. In addition, 33 bulk siliciclastic fraction samples from core BT-7 were also analyzed. Sediment samples were treated with acetic acid (25% v/v) and hydrogen peroxide (33% v/v) to remove carbonate and organic matter, respectively. Fractions <63 μm were obtained by sieving and fractions <2 μm were obtained following the same analytical procedure used to prepare samples for XRD clay mineralogy determination.

Initially, 50 mg of sub-samples were dissolved in 3 ml 40% hydrofluoric (HF)-300 μl 67% perchloric acid (HClO_4) mixtures and 3 ml 34% HCl-3 ml 67% HNO_3 mixtures, respectively. Separation of Sr and rare earth elements (REEs) was achieved using a Bio-Rad column packed with AG50WX-8, 200–400 mesh cationic exchange resin, and 2 N hydrochloric acid and 2.5 N nitric acid, respectively. The Sr fraction was further purified on a 20- μl SrSpec® column consisting of a polyethylene syringe with a 4 mm \varnothing Millex® filter (Colin et al., 2006). Nd was purified from the REEs by using TRU Spec and Ln-Spec resins following the analytical procedures described in Copard et al. (2010). The Sr and Nd isotopic compositions were measured using a Thermo Scientific Multi-Collector Induced Coupled Plasma Mass Spectrometer (MC-ICP-MS NEPTUNE Plus) located at the *Laboratoire des Sciences du Climat et de l'Environnement* (Gif-sur-Yvette, PANOPLY's analytical facilities at the Université Paris-Saclay, France). The samples and standard concentrations were matched at 20 ppb for the Nd and Sr isotope analyses. During the analytical processes, every three samples were bracketed with analyses of appropriate Sr standard solution NIST SRM987 ($^{87}\text{Sr}/^{86}\text{Sr} \approx 0.710250 \pm 0.000016$) and Nd standard solution JNdi-1 ($^{143}\text{Nd}/^{144}\text{Nd} \approx 0.512115$) (Lugmair et al., 1983; Tanaka et al., 2000). The Sr and Nd isotopic ratios were corrected from mass bias according to the exponential law relative to $^{146}\text{Nd}/^{144}\text{Nd} = 0.7219$ and $^{86}\text{Sr}/^{88}\text{Sr} = 0.1194$, respectively. The total procedural blanks for Nd and Sr are <30 pg, which represents <0.1% of the lowest quantity of Nd and Sr of samples, and thus can be ignored. The analytical error for each sample was taken as the external reproducibility of the La Jolla or NIST SRM987 standard unless the internal error was larger. For convenience, the Nd isotopic composition is expressed as $\epsilon\text{Nd}(0) = [({}^{143}\text{Nd}/{}^{144}\text{Nd})_{\text{sample}} / ({}^{143}\text{Nd}/{}^{144}\text{Nd})_{\text{CHUR}} - 1] \times 10,000$, with the present-day (${}^{143}\text{Nd}/{}^{144}\text{Nd}$)_{CHUR} of 0.512638 (Jacobsen & Wasserburg, 1980).

4. Results

4.1. Chronological Framework

As planktonic foraminifera are rare at the bottom of core CJB01-64, the age model of this core has been established using a Bayesian approach (Blaauw & Christen, 2011) based on five calibrated AMS ^{14}C dates measured on well-preserved calcareous test samples of mixed benthic foraminifera, gastropod shells, and the sample of plant debris (Figure S1 in Supporting Information S1; Table 1). Although this material is not good for ^{14}C dating as planktonic foraminifera, the use of this material is also acceptable, at least at the glacial/interglacial timescale from previous studies in this area (Hanebuth et al., 2003; Jiwaringrueangkul, Liu, Stattegger, & Sang, 2019; Jiwaringrueangkul, Liu, & Zhao, 2019). The established age model reveals that the upper 158 cm of core CJB01-64 extends back to 13.3 cal ka BP, with an average linear sedimentation rate of 11.8 cm/ka (varying from 10.6 to 21.1 cm/ka).

The age model of core CJB01-75 has also been established using a Bayesian approach (Blaauw & Christen, 2011) based on seven calibrated AMS ^{14}C dates obtained on mixed benthic foraminifera samples (Figure S1 in Supporting Information S1; Table 1). Core CJB01-75 provides a continuous record over the last 4.0 cal ka BP, with an average sedimentation rate of 37.3 cm/ka (from 41.7 to 329.1 cm/ka).

The age model of core BT-7 was established by Zhang et al. (2021) and was obtained by using seven calibrated AMS ^{14}C dates from benthic foraminifera and plant materials (Zhang et al., 2021). The age model of core BT-7 has been re-established using a Bayesian approach (Blaauw & Christen, 2011) in this study. Core BT-7 extends back to 12.8 cal ka BP, with an average sedimentation rate of 37.9 cm/ka.

4.2. Laser Grain-Size

The grain size composition of core BT-7 has been previously described by Zhang et al. (2021). Sediments from core CJB01-64 are dominated by silt (43%–73%) and clay (10%–33%), followed by sand (1%–46%) (Figure 2).

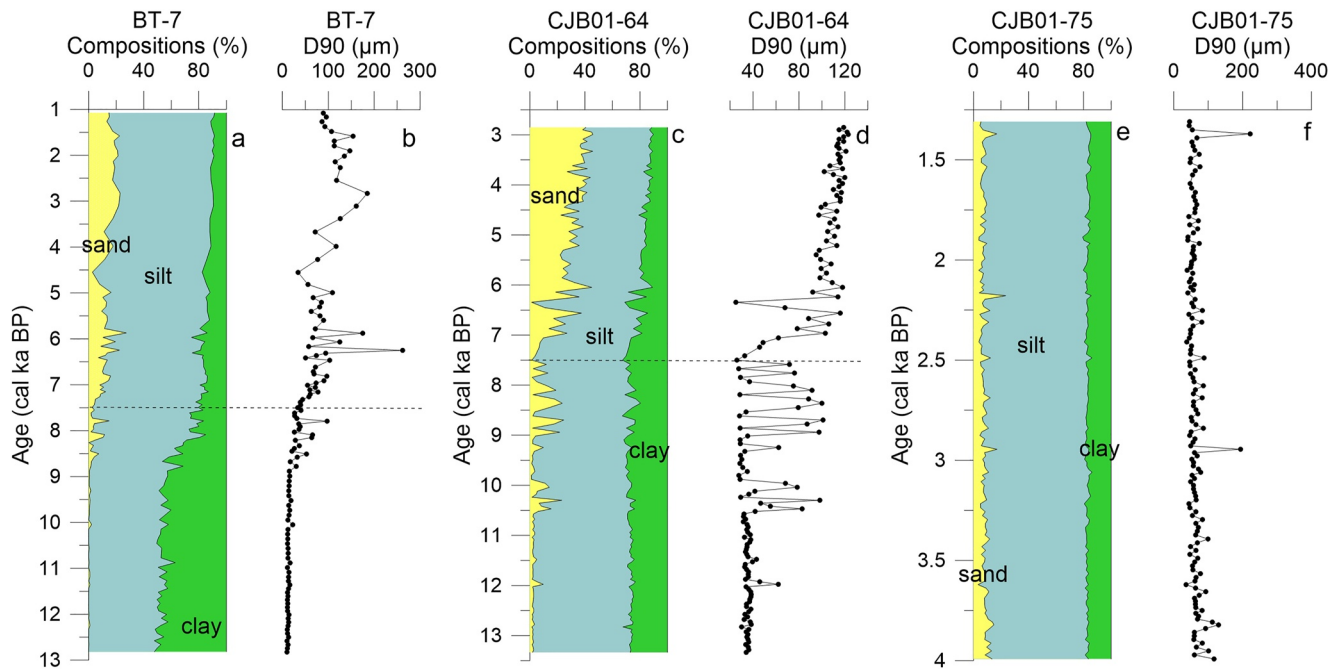


Figure 2. Variations in grain size (D90 (μm)) and proportions (%) of sand, silt, and clay obtained on cores. (a and b) Core BT-7 (Zhang et al., 2021) from the Gulf of Thailand. (c–f) Cores CJB01-64 and CJB01-75 from the central Sunda Shelf. The dashed lines at approximately 7.5 cal ka BP indicate the boundaries of the grain size transitions at these cores.

D90, which means that 90% of the total particles are smaller than this size, is used to represent the grain size distribution. Core CJB01-64 has grain size values (D90) ranging between 25 and 125 μm . The grain size (D90) and proportions of sand, silt, and clay display a significant change at around 7.5 cal ka BP with finer grain size (average 43 μm) before 7.5 cal ka BP than after (average 105 μm).

Core CJB01-75 sediments are mainly composed of silt (55%–80%) and clay (13%–21%), with a small amount of sand (3%–28%) (Figure 2). Except for 4 analytical results, the grain sizes (D90) display a narrow range from 36 to 130 μm . No coherent long-term change in grain size and proportions of sand, silt, and clay could be observed along the core.

4.3. Clay Mineralogical Compositions

4.3.1. Rivers of Thailand and the Malay Peninsula

Most rivers in the northern Gulf of Thailand have similar clay mineral compositions (Figure 3a). Clay mineral assemblages of northern Thailand rivers (Chao Phraya River, Mae Klong River, Tha Chin River, Bang Pakong River, and Pra Sea River) are characterized by high proportions of smectite (7%–65%, average 43%) and kaolinite (13%–75%, average 27%), with lesser amounts of illite (8%–28%, average 17%) and chlorite (7%–20%, average 13%) (Figure 3; Table 2). The clay mineral assemblages of the southern Thailand rivers (Tapi River and Pak Phanang River) are characterized by the dominance of kaolinite (33%–51%, average 42%), with lesser amounts of smectite (3%–41%, average 25%), illite (9%–29%, average 19%), and chlorite (9%–19%, average 14%) (Figure 3b).

The clay mineral assemblages of rivers on the Malay Peninsula are dominated by kaolinite (26%–78%, average 62%), followed by illite (15%–23%, average 20%) and chlorite (4%–42%, average 13%), with small amounts of smectite (0%–22%, average 5%) (Figure 3b).

4.3.2. Gulf of Thailand: Core BT-7

Clay mineral assemblages of core BT-7 are mainly composed of smectite (25%–57%, average 44%) and kaolinite (21%–30%, average 25%), with lesser amounts of chlorite (13%–21%, average 16%) and illite (8%–31%, average 15%) (Figure 4; Table S2 in Supporting Information S1). Except for kaolinite, clay mineral compositions since 13.3 cal ka BP display a significant change at around 7.5 cal ka BP (Figure 4). From 13.3 to 7.5 cal ka BP,

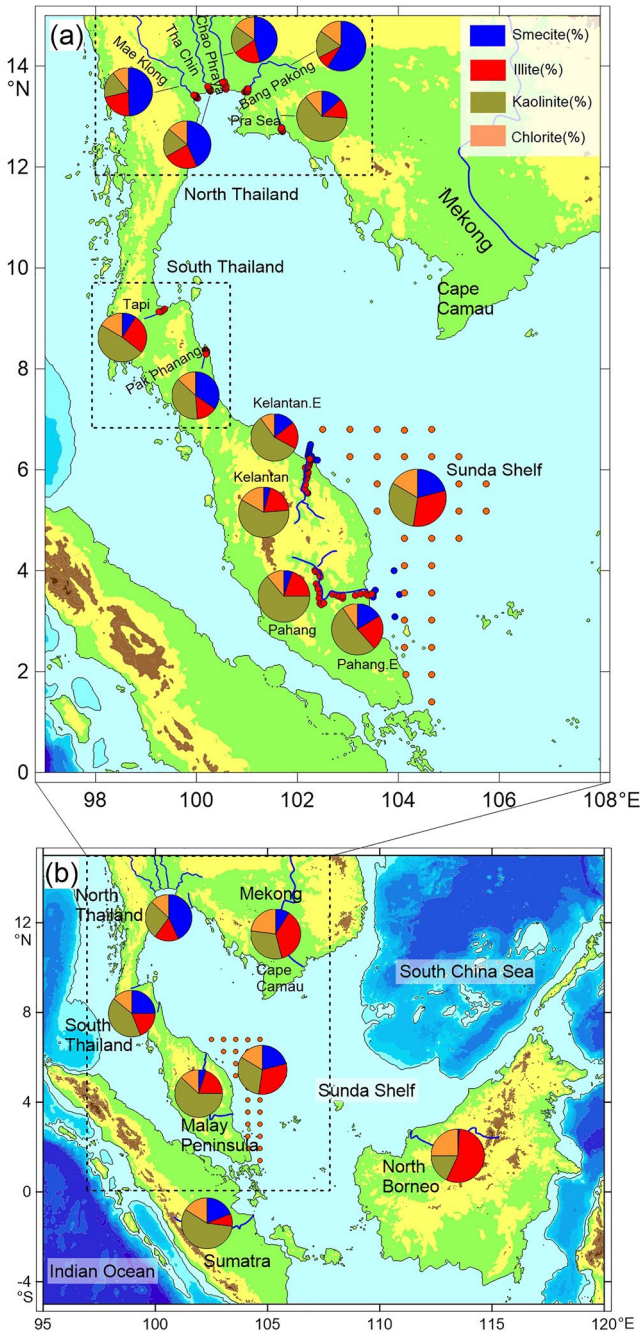


Figure 3. Clay mineral assemblages of rivers surrounding the Sunda Shelf. (a) Clay mineral assemblages of the river, estuary, and shelf sediments around Thailand and the Malay Peninsula. Kelantan, E: Kelantan estuary. Pahang, E: Pahang estuary. (b) Clay mineral provinces around the Sunda Shelf. The clay mineral compositions of the Mekong River and the rivers of Sumatra and Borneo are from Liu et al. (2016).

smectite contents decrease continuously (from 57% to 37%), whereas chlorite and kaolinite contents slightly increase from 13% to 21% and from 20% to 30%, respectively. No significant variations of illite contents (8%–14%, average 11%) can be observed during the time interval 13.3–7.5 cal ka BP. After 7.5 cal ka BP, illite increases abruptly and then increases continuously until 3 cal ka BP (from 11% to 31%), while smectite decreases (from 53% to 25%). Chlorite and kaolinite do not display any obvious variations (Figure 4).

4.3.3. Central Sunda Shelf: Surface Sediments and Cores CJB01-64 and CJB01-75

The clay mineral assemblages of estuaries located in the Malay Peninsula are dominated by kaolinite (33%–76%, average 55%), followed by illite (13%–27%, average 20%), smectite (0%–48%, average 15%), and chlorite (5%–16%, average 10%) (Figure 3a; Table S2 in Supporting Information S1). The clay mineral assemblages of sediments from the central Sunda Shelf are mainly composed of kaolinite (21%–70%, average 31%) and illite (21%–39%, average 31%), with lesser proportions of smectite (1%–38%, average 21%) and chlorite (8%–22%, average 16%). Smectite is enriched in the central shelf (Figure 5a). Illite and chlorite distributions show continuous enrichment from the offshore zone to the central shelf (Figures 5b and 5d). Kaolinite displays an opposite distribution compared to illite. Kaolinite displays the highest proportion in the offshore area and continuously decreases from the offshore to the central shelf (Figure 5c).

The clay mineral assemblages of core CJB01-64 are dominated by smectite (29%–66%, average 43%), followed by illite (12%–30%, average 22%), kaolinite (13%–23%, average 19%), and chlorite (9%–19%, average 15%) (Table S2 in Supporting Information S1). In general, illite, chlorite, and kaolinite variations are similar and display variations opposite to smectite variations. Since 13.3 cal ka BP, clay mineral compositions show an abrupt change at around 7.5 cal ka BP (Figure 6). Before 7.5 cal ka BP, smectite contents were low (29%–43%, average 34%) and thereafter increased until 4.5 cal ka BP (from 48% to 66%). The proportion of smectite is then constant after 4.5 cal ka BP. In contrast, illite, chlorite, and kaolinite contents are higher (22%–30%; 16%–19%; 18%–23%, respectively) before 7.5 cal ka BP and then decrease until 4.5 cal ka BP (from 21% to 12%; from 14% to 9%; from 18% to 13%, respectively) after 7.5 cal ka BP.

The clay mineral assemblages of core CJB01-75 are also dominated by smectite (57%–62%, average 59%), followed by kaolinite (14%–17%, average 16%), illite (14%–16%, average 15%), and chlorite (9%–11%, average 10%) (Table S2 in Supporting Information S1). No variations in clay mineral compositions occurred from 4.0 to 1.2 cal ka BP (Figure 6). It is worth noting that the percentage of each clay mineral of core CJB01-75 is similar to that of core CJB01-64 over the same time interval (Figure 6).

4.4. Sr-Nd Isotopic Compositions

$^{87}\text{Sr}/^{86}\text{Sr}$ ratios and ϵNd values analyzed on the bulk, $<63\ \mu\text{m}$, and clay-sized ($<2\ \mu\text{m}$) siliciclastic fractions from rivers, cores BT-7, CJB01-64, and CJB01-75 are listed in Table 2 and Figure 6.

4.4.1. Rivers Surrounding the Sunda Shelf

Except for the Mae Klong River, $^{87}\text{Sr}/^{86}\text{Sr}$ ratios and ϵNd values analyzed on two samples from each river investigated in this study showed similar isotopic compositions (Table 1). In addition, ϵNd values of sediment from the north Borneo river (MK16 and MK19) and from the Mekong River (samples MR04 and MR16) are consistent

Table 2
Sr and Nd Isotopic Compositions of Sediments From Cores CJB01-64, CJB01-75, and BT-7 in the Sunda Shelf, As Well As From Rivers Surrounding the Sunda Shelf

Cores	Latitude (°N)	Longitude (°E)	Depth in core (cm)	Age (cal a BP)	⁸⁷ Sr/ ⁸⁶ Sr < 63		¹⁴³ Nd/ ¹⁴⁴ Nd < 63		εNd < 3		⁸⁷ Sr/ ⁸⁶ Sr > 2		¹⁴³ Nd/ ¹⁴⁴ Nd < 2		εNd < 2	
					μm fraction	±2σ	μm fraction	±2σ	μm fraction	±2σ	μm fraction	±2σ	μm fraction	±2σ		
CJB01-64	6.00	104.97	5-6	2,973	0.72133	0.00001	0.512025	0.000006	-12.0	0.1	0.72885	0.00001	0.512079	0.000005	-10.9	0.1
CJB01-64	6.00	104.97	15-16	3,619	0.72130	0.00001	0.512033	0.000005	-11.8	0.1	0.72864	0.00001	0.512063	0.000005	-11.2	0.1
CJB01-64	6.00	104.97	25-26	4,265	0.72143	0.00001	0.512040	0.000005	-11.7	0.1	0.72843	0.00001	0.512065	0.000008	-11.2	0.2
CJB01-64	6.00	104.97	35-36	5,060	0.72304	0.00001	0.512048	0.000006	-11.5	0.1	0.72851	0.00001	0.512079	0.000007	-10.9	0.1
CJB01-64	6.00	104.97	45-46	6,005	0.72326	0.00001	0.512037	0.000005	-11.7	0.1	0.72823	0.00002	0.512087	0.000005	-10.8	0.1
CJB01-64	6.00	104.97	55-56	6,950	0.72313	0.00001	0.512041	0.000006	-11.6	0.1	0.72808	0.00001	0.512071	0.000007	-11.1	0.1
CJB01-64	6.00	104.97	65-66	7,820	0.72416	0.00001	0.512049	0.000006	-11.5	0.1	0.72776	0.00001	0.512079	0.000006	-10.9	0.1
CJB01-64	6.00	104.97	75-76	8,617	0.72424	0.00001	0.512042	0.000005	-11.6	0.1	0.72793	0.00001	0.512103	0.000011	-10.4	0.2
CJB01-64	6.00	104.97	85-86	9,414	0.72422	0.00001	0.512056	0.000005	-11.3	0.1	0.72766	0.00001	0.512076	0.000006	-11.0	0.1
CJB01-64	6.00	104.97	95-96	10,211	0.72353	0.00001	0.512047	0.000006	-11.5	0.1	0.72708	0.00001	0.512096	0.000007	-10.6	0.1
CJB01-64	6.00	104.97	105-106	10,686	0.72362	0.00001	0.512048	0.000005	-11.5	0.1	0.72783	0.00001	0.512083	0.000006	-10.8	0.1
CJB01-64	6.00	104.97	115-116	11,160	0.72346	0.00001	0.512044	0.000006	-11.6	0.1	0.72792	0.00001	0.512072	0.000006	-11.0	0.1
CJB01-64	6.00	104.97	125-126	11,635	0.72354	0.00001	0.512046	0.000005	-11.5	0.1	0.72791	0.00001	0.512081	0.000006	-10.9	0.1
CJB01-64	6.00	104.97	135-136	12,109	0.72346	0.00001	0.512037	0.000006	-11.7	0.1	0.72709	0.00001	0.512088	0.000005	-10.7	0.1
CJB01-64	6.00	104.97	145-146	12,584	0.72358	0.00001	0.512046	0.000007	-11.6	0.1	0.72706	0.00001	0.512098	0.000005	-10.5	0.1
CJB01-64	6.00	104.97	155-156	13,058	0.72393	0.00001	0.512059	0.000005	-11.3	0.1	0.72732	0.00001	0.512095	0.000003	-10.6	0.1
CJB01-75	4.91	105.53	5-6	1,351	0.72557	0.00001	0.512044	0.000005	-11.6	0.1	0.72940	0.00001	0.512071	0.000007	-11.1	0.1
CJB01-75	4.91	105.53	15-16	1,595	0.72556	0.00001	0.512030	0.000006	-11.9	0.1	0.72952	0.00001	0.512069	0.000006	-11.1	0.1
CJB01-75	4.91	105.53	20-21	1,717	0.72518	0.00001	0.512037	0.000006	-11.7	0.1	0.72929	0.00001	0.512063	0.000008	-11.2	0.2
CJB01-75	4.91	105.53	35-36	1,991	0.72577	0.00001	0.512047	0.000005	-11.5	0.1	0.72922	0.00001	0.512082	0.000008	-10.8	0.2
CJB01-75	4.91	105.53	45-46	2,053	0.72575	0.00001	0.512031	0.000006	-11.8	0.1	0.72937	0.00001	0.512075	0.000008	-11.0	0.2
CJB01-75	4.91	105.53	55-56	2,203	0.72578	0.00001	0.512043	0.000006	-11.6	0.1	0.72922	0.00001	0.512065	0.000008	-11.2	0.2
CJB01-75	4.91	105.53	65-66	2,443	0.72568	0.00001	0.512043	0.000005	-11.6	0.1	0.72917	0.00001	0.512075	0.000008	-11.0	0.2
CJB01-75	4.91	105.53	75-76	2,683	0.72544	0.00001	0.512033	0.000004	-11.8	0.1	0.72911	0.00001	0.512073	0.000009	-11.0	0.2
CJB01-75	4.91	105.53	85-86	2,868	0.72560	0.00002	0.512041	0.000006	-11.7	0.1	0.72920	0.00001	0.512073	0.000008	-11.0	0.2
CJB01-75	4.91	105.53	95-96	2,997	0.72612	0.00001	0.512046	0.000006	-11.5	0.1	0.72912	0.00001	0.512075	0.000009	-11.0	0.2
CJB01-75	4.91	105.53	105-106	3,167	0.72561	0.00001	0.512041	0.000005	-11.6	0.1	0.72909	0.00001	0.512086	0.000008	-10.8	0.2
CJB01-75	4.91	105.53	115-116	3,398	0.72543	0.00001	0.512028	0.000005	-11.9	0.1	0.72914	0.00001	0.512082	0.000008	-10.9	0.2
CJB01-75	4.91	105.53	125-126	3,629	0.72584	0.00001	0.512042	0.000005	-11.6	0.1	0.72911	0.00001	0.512079	0.000008	-10.9	0.2
CJB01-75	4.91	105.53	135-136	3,699	0.72549	0.00001	0.512045	0.000005	-11.6	0.1	0.72906	0.00001	0.512079	0.000008	-10.9	0.2
CJB01-75	4.91	105.53	145-146	3,730	0.72538	0.00002	0.512051	0.000005	-11.4	0.1	0.72909	0.00001	0.512082	0.000008	-10.8	0.2
MR04	10.24	106.37	Mekong R. (Indochina)		0.72113	0.00001	0.512134	0.000008	-9.8	0.2	0.72125	0.00001	0.512161	0.000011	-9.3	0.2
MR16	9.74	106.07	Mekong R. (Indochina)		0.72077	0.00001	0.512120	0.000008	-10.1	0.2	0.72122	0.00001	0.512153	0.000011	-9.5	0.2
MK16	2.28	111.81	Rajang R. (Borneo)		0.71992	0.00001	0.512245	0.000008	-7.7	0.2	0.71845	0.00001	0.512292	0.000011	-6.8	0.2
MK19	2.11	112.16	Rajang R. (Borneo)		0.71879	0.00001	0.512273	0.000009	-7.1	0.2	0.71866	0.00001	0.512302	0.000011	-6.5	0.2

Table 2
Continued

Cores	Latitude (°N)	Longitude (°E)	Depth in core (cm)	Age (cal a BP)	$^{87}\text{Sr}/^{86}\text{Sr} < 63$ µm fraction	$^{143}\text{Nd}/^{144}\text{Nd} < 63$ µm fraction	$^{143}\text{Nd}/^{144}\text{Nd} < 63$ ±2σ	$^{87}\text{Sr}/^{86}\text{Sr} > 2$ µm fraction	$^{87}\text{Sr}/^{86}\text{Sr} > 2$ ±2σ	$^{143}\text{Nd}/^{144}\text{Nd}$ <2 µm fraction	$^{143}\text{Nd}/^{144}\text{Nd}$ ±2σ	$\epsilon_{\text{Nd}} < 2$ µm fraction	$\epsilon_{\text{Nd}} < 2$ ±2σ
SU08	-1.58	103.57	Hari R. (Sumatra)		0.71158	0.00001	0.512409	0.000008	0.2	0.512480	0.000007	-3.1	0.1
SU09	-1.71	103.25	Hari R. (Sumatra)		0.71053	0.00001	0.512400	0.000008	0.2	0.512481	0.000007	-3.1	0.1
Chao-1	13.54	100.58	Chao Phraya R. (Thailand)		0.72056	0.00001	0.512117	0.000008	0.2	0.512138	0.000007	-9.8	0.1
Chao-2	13.57	100.57	Chao Phraya R. (Thailand)		0.72047	0.00001	0.512151	0.000011	0.2	0.512165	0.000007	-9.2	0.1
MK-1	13.36	100.02	Mae Klong R. (Thailand)		0.73903	0.00001	0.511916	0.000011	0.2	0.511957	0.000007	-13.3	0.1
KR-2	6.21	102.24	Kelantan R. (Malay Peninsula)		0.72395	0.00001	0.512233	0.000011	0.2	0.512253	0.000007	-7.5	0.1
KR-4	6.19	102.26	Kelantan R. (Malay Peninsula)		0.72466	0.00001	0.512218	0.000011	0.2	0.512235	0.000005	-7.9	0.1

Cores	Latitude (°N)	Longitude (°E)	Depth in the core (cm)	Age (cal a BP)	$^{87}\text{Sr}/^{86}\text{Sr}$ bulk fraction	$^{143}\text{Nd}/^{144}\text{Nd}$ bulk fraction	$^{143}\text{Nd}/^{144}\text{Nd}$ ±2σ	ϵ_{Nd} bulk fraction	±2σ	Samples	River	Latitude (°N)	Longitude (°E)	$\epsilon_{\text{Nd}} < 63$ µm fraction	Data source
BT-7	9.11	100.92	4-6	1,465	0.72382	0.00001	0.512071	0.000003	0.1	MR04	Mekong R. (Indochina)	10.24	106.37	-10.2	Liu et al. (2007)
BT-7	9.11	100.92	16-18	2,941	0.72202	0.00001	0.512072	0.000003	0.1	MR16	Mekong R. (Indochina)	9.74	106.07	-10.5	Liu et al. (2007)
BT-7	9.11	100.92	22-26	3,237	0.72285	0.00001	0.512046	0.000003	0.1	MK16	Rajang R. (Borneo)	2.28	111.81	-7.7	Liu et al. (2016)
BT-7	9.11	100.92	36-38	3,682	0.72469	0.00001	0.512062	0.000003	0.1	MK19	Rajang R. (Borneo)	2.11	112.16	-7.1	Liu et al. (2016)
BT-7	9.11	100.92	52-54	4,274	0.72566	0.00001	0.512055	0.000003	0.1						
BT-7	9.11	100.92	64-66	4,719	0.72553	0.00000	0.512058	0.000002	0.0						
BT-7	9.11	100.92	72-74	5,015	0.72573	0.00001	0.512048	0.000004	0.1						
BT-7	9.11	100.92	84-86	5,441	0.72614	0.00000	0.512040	0.000002	0.0						
BT-7	9.11	100.92	92-94	5,661	0.72558	0.00001	0.512042	0.000004	0.1						
BT-7	9.11	100.92	112-114	6,212	0.72419	0.00001	0.512038	0.000003	0.1						
BT-7	9.11	100.92	128-130	6,653	0.72868	0.00001	0.512006	0.000003	0.1						
BT-7	9.11	100.92	140-142	6,898	0.72824	0.00001	0.511995	0.000002	0.0						
BT-7	9.11	100.92	164-166	7,050	0.72921	0.00001	0.511980	0.000002	0.0						
BT-7	9.11	100.92	180-182	7,151	0.72921	0.00001	0.511996	0.000003	0.1						
BT-7	9.11	100.92	188-190	7,201	0.72866	0.00001	0.511995	0.000003	0.1						
BT-7	9.11	100.92	196-198	7,252	0.72925	0.00001	0.511999	0.000003	0.1						
BT-7	9.11	100.92	200-202	7,277	0.72820	0.00001	0.511997	0.000003	0.1						
BT-7	9.11	100.92	208-210	7,327	0.72946	0.00001	0.511994	0.000003	0.1						
BT-7	9.11	100.92	220-222	7,441	0.72781	0.00001	0.512000	0.000003	0.1						
BT-7	9.11	100.92	228-230	7,543	0.72763	0.00001	0.512006	0.000003	0.1						

Table 2
Continued

Cores	Latitude (°N)	Longitude (°E)	Depth in the core (cm)	Age (cal a BP)	⁸⁷ Sr/ ⁸⁶ Sr bulk fraction	¹⁴³ Nd/ ¹⁴⁴ Nd bulk fraction	±2σ	εNd bulk fraction	±2σ	Samples	River	Latitude (°N)	Longitude (°E)	εNd <63 μm fraction	Data source
BT-7	9.11	100.92	256–258	7,900	0.72527	0.512031	0.00001	−11.8	0.000003	0.1					
BT-7	9.11	100.92	268–270	8,053	0.72540	0.512029	0.00001	−11.9	0.000003	0.1					
BT-7	9.11	100.92	280–282	8,205	0.72689	0.511990	0.00002	−12.7	0.000003	0.1					
BT-7	9.11	100.92	292–294	8,358	0.72844	0.512006	0.00001	−12.3	0.000002	0.0					
BT-7	9.11	100.92	312–314	8,750	0.72897	0.512006	0.00001	−12.3	0.000002	0.0					
BT-7	9.11	100.92	344–346	9,597	0.72749	0.512037	0.00001	−11.7	0.000004	0.1					
BT-7	9.11	100.92	384–386	10,655	0.72825	0.512035	0.00001	−11.8	0.000003	0.1					
BT-7	9.11	100.92	396–398	10,972	0.72849	0.512027	0.00001	−11.9	0.000003	0.1					
BT-7	9.11	100.92	428–430	11,819	0.72798	0.512032	0.00001	−11.8	0.000003	0.1					
BT-7	9.11	100.92	436–438	12,031	0.72910	0.512027	0.00001	−11.9	0.000002	0.0					
BT-7	9.11	100.92	452–454	12,454	0.72796	0.512013	0.00001	−12.2	0.000002	0.0					
BT-7	9.11	100.92	472–474	12,983	0.72872	0.512024	0.00001	−12.0	0.000002	0.0					
BT-7	9.11	100.92	484–486	13,300	0.72828	0.512033	0.00001	−11.8	0.000005	0.1					

Note. εNd (0) = [(¹⁴³Nd/¹⁴⁴Nd)_{sample} / (¹⁴³Nd/¹⁴⁴Nd)_{CHUR} − 1] × 10,000, and (¹⁴³Nd/¹⁴⁴Nd)_{CHUR} = 0.512638 (Jacobsen & Wasserburg, 1980). R. = river, for example, Mekong R. = Mekong River.

with the previously published values for river sediments from the same sampling sites and the same size fractions (<63 μm) (−7.7 for MK16 and −7.1 for MK19 of Borneo rivers and −10.5 for MR16 and −10.2 for MR04 of Mekong River) (Table 2; Liu et al., 2007, 2016).

For the <63 μm fraction, the Mekong River (mean εNd of −10.0 and ⁸⁷Sr/⁸⁶Sr ratio of 0.7209), the Rajang River in Borneo (mean εNd of −7.4 and ⁸⁷Sr/⁸⁶Sr ratio of 0.7193), the Hari River in Sumatra (mean εNd of −4.8 and ⁸⁷Sr/⁸⁶Sr ratio of 0.7110), and the Kelantan River of the Malay Peninsula (mean εNd of −8.0 and ⁸⁷Sr/⁸⁶Sr ratio of 0.7193) display different ⁸⁷Sr/⁸⁶Sr ratios and εNd values (Table 2). Samples from the Chao Phraya River (εNd of −9.5 and ⁸⁷Sr/⁸⁶Sr ratio of 0.7205) and Mae Kong River (εNd of −14.1 and ⁸⁷Sr/⁸⁶Sr ratio of 0.7390) in Thailand display contrasted εNd values and ⁸⁷Sr/⁸⁶Sr ratios in agreement with the contrasted lithology of the regions drained by these two rivers.

⁸⁷Sr/⁸⁶Sr ratios and εNd obtained on the <2 μm fraction are also reported in Table 2 and are consistent with the Sr and Nd isotopic compositions obtained on <63 μm fraction with some slight deviations. These deviations, which have already been revealed in many previous studies comparing Sr and Nd isotopic analyses of different grain-sizes of the sediments, are due to different mineralogical compositions (Bayon et al., 2015; Carter et al., 2020; Jonell et al., 2018).

4.4.2. Gulf of Thailand: Core BT-7

For core BT-7, the εNd values range from −12.8 to −11.0, and ⁸⁷Sr/⁸⁶Sr ratios range from 0.7220 to 0.7295. A significant change in the εNd values and ⁸⁷Sr/⁸⁶Sr occurs at around 7.5 cal ka BP: sediments from the 13.3–7.5 cal ka BP time interval are characterized by lower radiogenic εNd (between −12.7 and −11.7) than sediments from the 7.5 to 0 cal ka BP time interval (between −12.8 and −11.0); ⁸⁷Sr/⁸⁶Sr ratios of the 13.3–7.5 cal ka BP period are higher (0.7253–0.7291) than those of the 7.5–0 cal ka BP period (0.7220–0.7294) (Figure 4; Table 2).

4.4.3. Central Sunda Shelf: Cores CJB01-64 and CJB01-75

For core CJB01-64, <63 μm fractions yield εNd values ranging from −11.9 to −11.3 and ⁸⁷Sr/⁸⁶Sr ratios from 0.7213 to 0.7242. Similar to the Gulf of Thailand, significant changes in εNd values and ⁸⁷Sr/⁸⁶Sr ratios are also observed at 7.5 cal ka BP. During the 13.3–7.5 cal ka BP period, εNd and ⁸⁷Sr/⁸⁶Sr are higher (εNd = −11.7 to −11.3; ⁸⁷Sr/⁸⁶Sr = 0.7235–0.7242) than those of the time interval 7.5–2.6 cal ka BP (εNd = −12.0 to −11.5; ⁸⁷Sr/⁸⁶Sr = 0.7213–0.7233) (Figure 6; Table 2). For <2 μm fractions, εNd values range from −11.2 to −10.4, and ⁸⁷Sr/⁸⁶Sr ratios are characterized by a narrow range from 0.7271 to 0.7288. εNd and ⁸⁷Sr/⁸⁶Sr ratios also display significant changes at 7.5 cal ka BP. The time interval from 13.3 to 7.5 cal ka BP is characterized by higher radiogenic εNd (between −11.0 and −10.4) than the time interval from 7.5 to 2.6 cal ka BP (from −11.2 to −10.8). This is associated with lower ⁸⁷Sr/⁸⁶Sr ratios (0.7271–0.7279) for the period 13.3–7.5 cal ka BP than those for the period 7.5–2.6 cal ka BP (0.7281–0.7288) (Figure 6; Table 2).

For core CJB01-75, εNd values and ⁸⁷Sr/⁸⁶Sr ratios of the <63 μm fraction display a narrow range from −11.9 to −11.5 and from 0.7252 to 0.7261, respectively (Figure 6; Table 2). εNd values and ⁸⁷Sr/⁸⁶Sr ratios display no

variations during the last 4.0 cal ka BP (Figure 6). Core CJB01-75 has higher $^{87}\text{Sr}/^{86}\text{Sr}$ and ϵNd values in the $<63\ \mu\text{m}$ fraction than core CJB01-64. For the $<2\ \mu\text{m}$ fractions, ϵNd values and $^{87}\text{Sr}/^{86}\text{Sr}$ ratios both also have a narrow range from -11.2 to -10.8 and from 0.7291 to 0.7295 , respectively. ϵNd values and $^{87}\text{Sr}/^{86}\text{Sr}$ signatures have similar isotopic compositions (within the error) to core CJB01-64 over the same time interval (Figure 6).

5. Discussion

5.1. Sediment Sources of the Gulf of Thailand and the Central Sunda Shelf

5.1.1. Sr-Nd Isotopic Evidence

The $^{87}\text{Sr}/^{86}\text{Sr}$ ratios versus ϵNd measured for the decarbonated sediments of core BT-7 and the $<63\ \mu\text{m}$ fraction of cores CJB01-64 and CJB01-75 are presented in Figure 7a, together with data for core T93 sediments in the Gulf of Thailand and river sediments looked at in this study and those previously reported by Liu et al. (2007) and Chen (2020). Sr-Nd isotopic ranges for tectonic terranes are also plotted in Figure 7a. The tectonic terranes and corresponding river drainage sediment display similar isotopic compositions, especially for Nd isotopes, although Sr isotopes show a slight offset between the Malay Peninsula rivers and the potential basement (Sibumasu Block). Based on this, the isotopic composition of river sediments could be used as end members. In Figure 7b, more detailed data are presented for the sediments from the periods 13.3–7.5 and 7.5–0 cal ka BP. In these diagrams, the mixing of sediments from every two different sources generates a hyperbolic trend between the end members. As the sources of Borneo rivers are located south of these cores, they are excluded from a significant contribution of sediment. This is in agreement with previous observations suggesting that sediments from Borneo's rivers are mainly deposited over the offshore area (Staub & Gastaldo, 2000).

5.1.1.1. Sediment Sources of the Gulf of Thailand: Core BT-7

Sr and Nd isotopic compositions obtained on the decarbonated sediments of core BT-7 mainly fit along a mixing curve between two end members (Figures 7a and 7b). One of these corresponds to the isotopic composition of sediment recovered from the Mekong River/Chao Phraya River. The second end member corresponds to that of the Mae Klong River (northern Thailand).

The Mekong River and Chao Phraya River end members overlap, indicating their isotopic similarity. The upper reaches of the Chao Phraya River are mainly composed of Paleozoic-Mesozoic sedimentary rocks, and the bedrock of the lower reaches is dominated by Quaternary deposits (Figure 1). The basement in the upper reaches of the Mekong River consists mainly of Mesozoic sedimentary rocks, the middle reaches are underlain mainly by Paleozoic-Mesozoic sedimentary rocks and Paleozoic-Cenozoic granitic rocks, and the lower reaches are mainly Quaternary deposits (Liu et al., 2004). Therefore, these two river drainage basins have similar stratigraphy with Paleozoic-Mesozoic sedimentary rocks in the middle-upper reaches and Quaternary deposits in the lower reaches, which could lead to their similar isotopic compositions. Although the Mae Klong River and Chao Phraya River are both located in northern Thailand, these two river basins have different geological formations (Figure 1), a fact that explains their isotopic differences. Additionally, the sediment discharge rate of the Mae Klong River (8.1 Mt/yr) is comparable to that of the Chao Phraya River (11 Mt/yr) (Table S1 in Supporting Information S1). Thus, the Mae Klong River is an important end member.

Since these study cores are also plotted on the mixing line of the Sumatra and Thailand (Mae Klong River) end members, Sumatra sediment may influence these cores. Weathering of the basaltic region produces a large amount of smectite, which can result in smectite making up 90%–95% of the clay-size fraction under seasonal subtropical conditions (Liu et al., 2009). Although Sumatra is characterized by a tropical climate and smectite content only accounts for 19% of the volume content of all clay minerals (Liu et al., 2016), Sumatra has the relatively highest smectite content in the southern part of the Sunda Shelf. If smectite on the Sunda Shelf derives from the basaltic province of Sumatra or the Mekong River basin, an increase in smectite contents would be associated with a decrease in the $^{87}\text{Sr}/^{86}\text{Sr}$ ratios and an increase in ϵNd values. Figure 8 presents the $^{87}\text{Sr}/^{86}\text{Sr}$ ratios and ϵNd versus each clay mineral content for samples from cores BT-7 and CJB01-64. $^{87}\text{Sr}/^{86}\text{Sr}$ ratios and smectite contents of core BT-7 display positive correlations ($R^2 = 0.41$, $P < 0.01$) (Figure 8a), and ϵNd values and smectite contents display weak negative correlations ($R^2 = 0.17$, $P < 0.05$) (Figure 8c). Therefore, the smectite of core BT-7 could not derive from Sumatra's Rivers but must instead derive mainly from the Mae Klong River, which is

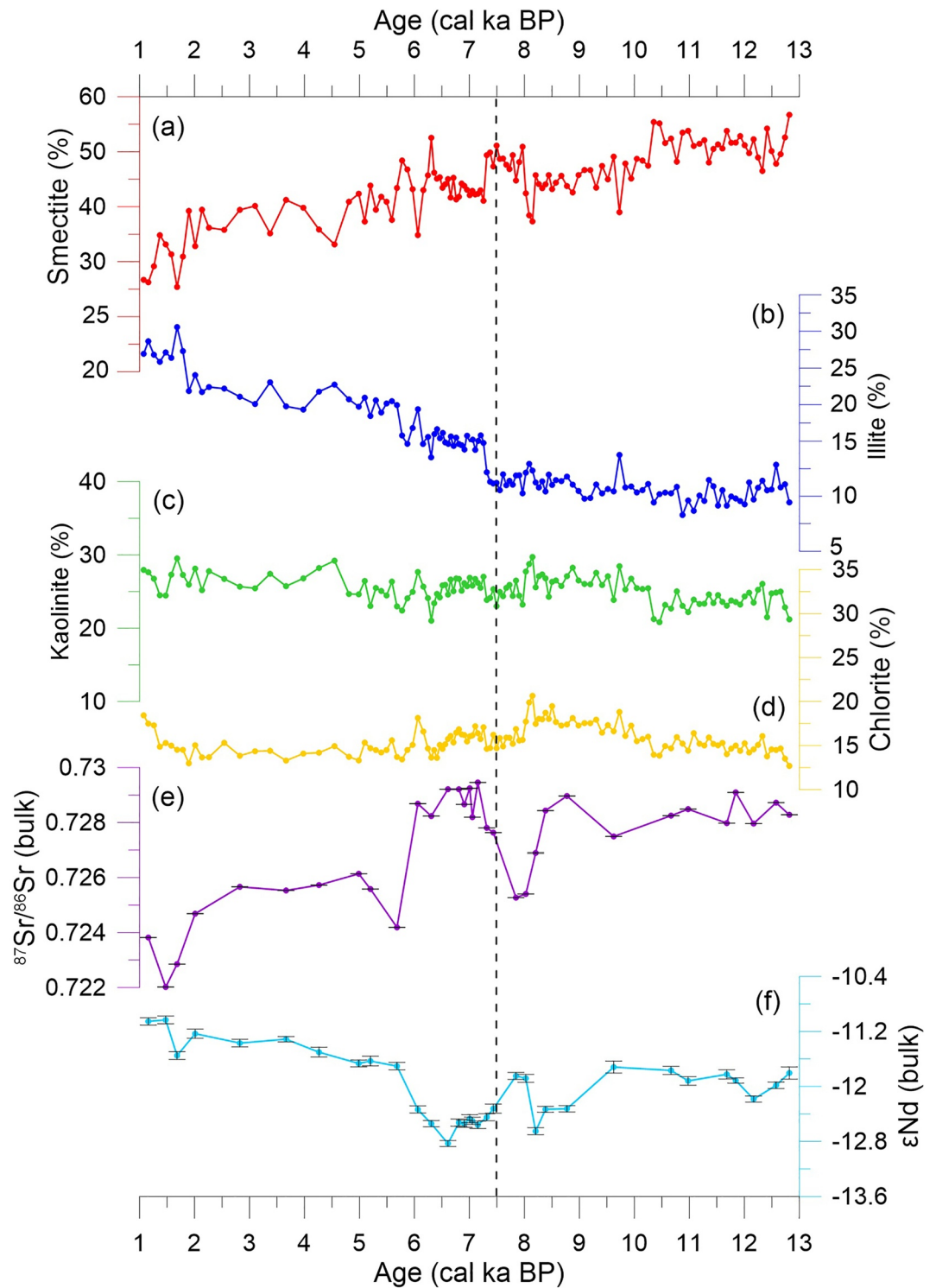


Figure 4. Clay mineral and Sr-Nd isotopic variations of core BT-7 in the Gulf of Thailand (in the northern Sunda Shelf) since the last deglaciation. (a–d) Clay mineral variations of core BT-7. (e and f) Sr-Nd isotopic variations of core BT-7. The dashed line at approximately 7.5 cal ka BP indicates the boundaries of the clay mineral and Sr-Nd isotopic transitions at core BT-7.

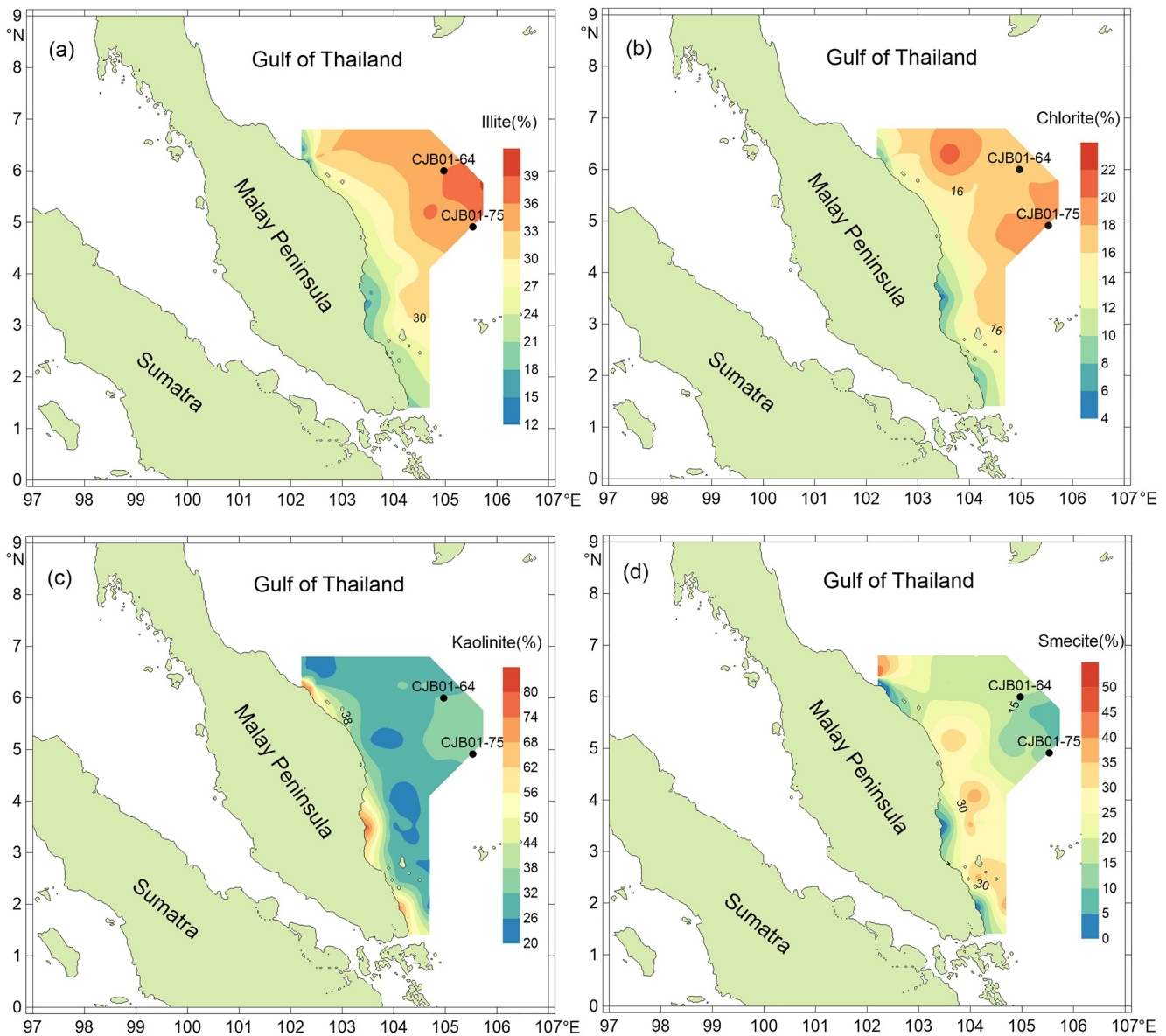


Figure 5. The spatial distribution of clay mineral percentages in the central Sunda Shelf off the Malay Peninsula. (a) Illite. (b) Chlorite. (c) Kaolinite. (d) Smectite. The kriging method was used to perform the interpolations with the clay data.

characterized by high smectite contents (from 41% to 55%) (Wu, 2023), as well as high $^{87}\text{Sr}/^{86}\text{Sr}$ ratios (0.7390) and low ϵNd values (-14.1) (Figure 7). Negative correlations between illite contents and $^{87}\text{Sr}/^{86}\text{Sr}$ ratios of core BT-7 ($R^2 = 0.58$, $P < 0.01$) (Figure 8b) and positive correlations between illite contents and ϵNd values ($R^2 = 0.36$, $P < 0.01$) (Figure 8d) suggest that higher illite contents correspond to lower $^{87}\text{Sr}/^{86}\text{Sr}$ ratios and higher ϵNd values. The Mekong River, characterized by high illite contents, as well as lower $^{87}\text{Sr}/^{86}\text{Sr}$ ratios (0.7203–0.7222) and higher ϵNd values (-10.1 to -9.8) (Liu et al., 2007), is therefore likely to be the main source of illite.

The isotopic characteristics suggest that sediments deposited during the 13.3–7.5 cal ka BP interval are derived from the mixing of Mekong River and Mae Klong River end members (Figure 7b), with a 50%–60% contribution from the Mekong River end member. For the 7.5–0 cal ka BP period, the samples are closer to the Mekong River end member, suggesting a greater contribution from the Mekong River (65%–90%) to the Gulf of Thailand after 7.5 cal ka BP. Although the Sr isotopes could be influenced by chemical weathering, the Nd isotope is not affected by weathering and it is closer to the Mekong River end member (Figure 7b). Sediments deposited off Cape Camau, close to the Gulf of Thailand, have similar Sr and Nd isotopic compositions to the Mekong River

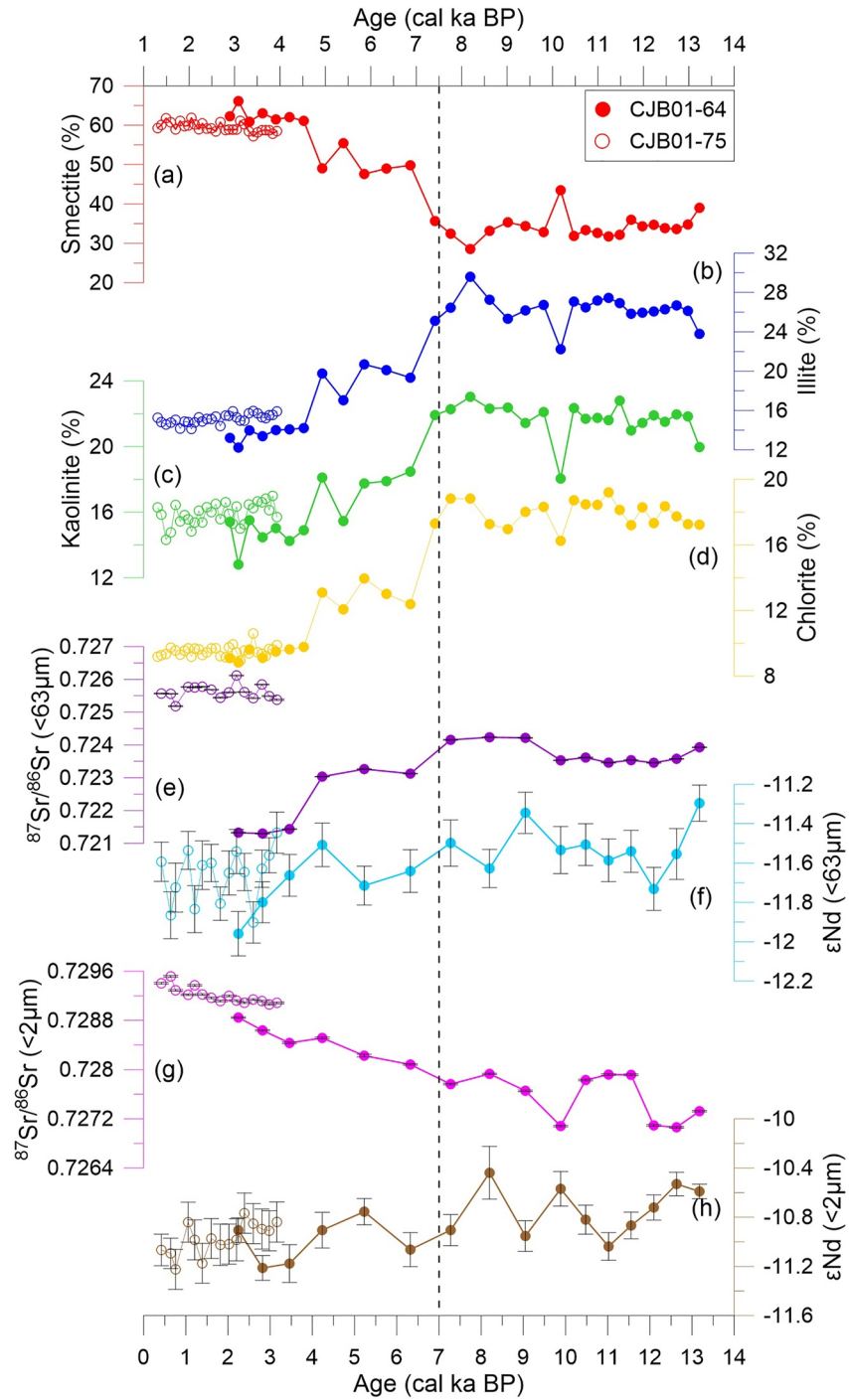


Figure 6. Clay mineral and Sr-Nd isotopic variations of cores CJB01-64 and CJB01-75 in the central Sunda Shelf since the last deglaciation. (a–d) Clay mineral variations of two cores. (e–h) Sr-Nd isotopic variations of <63 and <2 μm fractions of two cores. Solid circles and hollow circles represent cores CJB01-64 and CJB01-75, respectively. The dashed line at approximately 7.5 cal ka BP indicates the boundaries of the clay mineral and Sr-Nd isotopic transitions at core CJB01-64.

(Chen, 2020), indicating that sediment in Cape Camau is transported from the Mekong River (Xue et al., 2010). Core T93, from the Gulf of Thailand close to core BT-7, shares similar Sr and Nd isotopic distributions and variation trends with core BT-7 for the 13.3–7.5 cal ka BP and 7.5–0 cal ka BP time intervals (Figure 7b). Thus, the Gulf of Thailand received higher sediment contributions from the Mekong River after 7.5 cal ka BP.

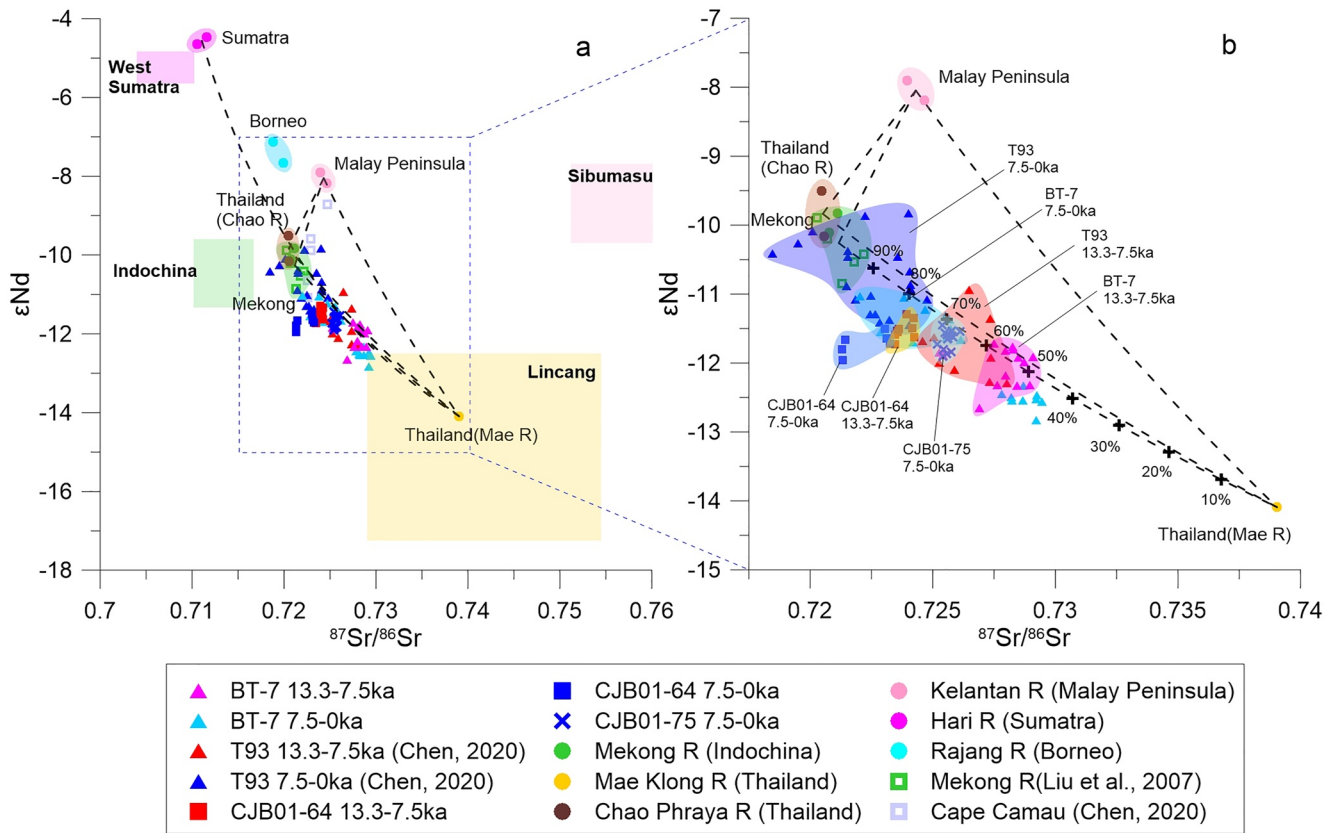


Figure 7. $^{87}Sr/^{86}Sr$ ratios versus ϵ_{Nd} diagram. (a) $^{87}Sr/^{86}Sr$ ratios versus ϵ_{Nd} diagram for samples from cores BT-7 and T93 (Chen, 2020) (decarbonated sediments) from the Gulf of Thailand and cores CJB01-64 and CJB01-75 (<63 μ m fractions) from the central Sunda Shelf, potential river end members represented by ellipses (<63 μ m fractions), including the Mekong River (Liu et al., 2007 and this study), Chao Phraya River (Thailand), Mae Klong River (Thailand), Kelantan River (Malay Peninsula), Batang Hari River (Sumatra), and Rajang River (Borneo), and tectonic terranes represented by rectangles, including Indochina (Lan et al., 2003), Sibumasu (Jiang et al., 2017), west Sumatra (Zhang et al., 2020), and Lincang (Deng et al., 2018) terranes (see Figure 1c). (b) A zoomed-in detail of (a) to show sediment source variations of two periods (e.g., 13.3–7.5 ka and 7.5–0 ka) in the Gulf of Thailand and central Sunda Shelf. The concentrations of Sr and Nd used to calculate the mixing of sediments are from Liu et al. (2007) (Mekong River), Qiao et al. (2015) (Chao Phraya River and Mae Klong River), Wu et al. (2019, 2022) (Kelantan River), Liu et al. (2016) (Hari River). Thailand (Chao R) = Chao Phraya River in Thailand, Thailand (Mae R) = Mae Klong River in Thailand.

5.1.1.2. Sediment Sources of the Central Sunda Shelf: Cores CJB01-64 and CJB01-75

As for the core located in the Gulf of Thailand (BT-7), there were positive correlations between smectite contents and $^{87}Sr/^{86}Sr$ ratios of core CJB01-64 ($R^2 = 0.54$, $P < 0.01$) (Figure 8a), and weak negative correlations between smectite contents and ϵ_{Nd} values ($R^2 = 0.28$, $P < 0.05$) (Figure 8c). This indicates that the smectite in core CJB01-64 does not derive from the weathering of volcanic rock in the Sumatra River basin but probably also derives mainly from the Mae Klong River. In addition, negative correlations between $^{87}Sr/^{86}Sr$ ratios and illite contents of core CJB01-64 ($R^2 = 0.53$, $P < 0.01$) (Figure 8b) and positive correlations between ϵ_{Nd} values and illite contents ($R^2 = 0.30$, $P < 0.05$) (Figure 8d) suggest that the illite derives mainly from the Mekong River basin.

Sr and Nd isotopic compositions obtained on the <63 μ m sediment fraction of core CJB01-64 also mainly fit along a mixing curve between the Mekong River and Mae Klong River end members (Figure 7b). It seems that the Mekong River end member has higher sediment contributions during the 7.5–0 cal ka BP period (80%–90%) than 13.3–7.5 cal ka BP (70%–80%) of core CJB01-64. The samples of 7.5–0 cal ka BP period of core CJB01-64 are not located on the mixing curve between the Mekong River and Mae Klong River end members. For the $^{87}Sr/^{86}Sr$ values, the samples are closer to the source of the Mekong/Chao Phraya River. However, for the ϵ_{Nd} values, the samples are slightly closer to the source of the Mae Klong River. The Nd isotope is more reliable in tracing the provenance compared to the Sr isotope. Therefore, we suggest that the samples of 7.5–0 cal ka BP are slightly closer to the Mae Klong River end member.

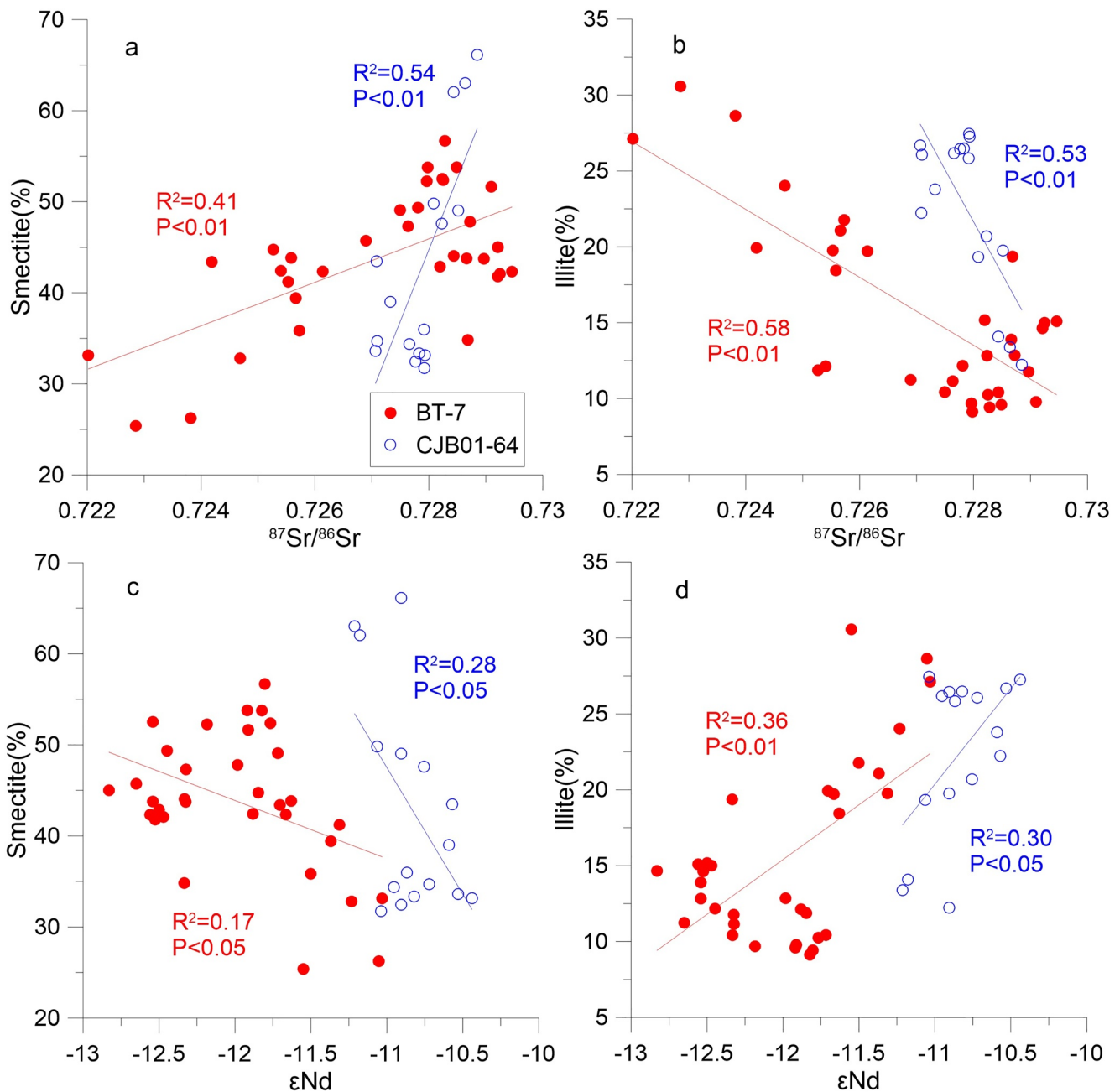


Figure 8. $^{87}\text{Sr}/^{86}\text{Sr}$ and ϵNd compositions versus smectite and illite contents for samples from core BT-7 in the Gulf of Thailand and core CJB01-64 in the central Sunda Shelf. (a and b) $^{87}\text{Sr}/^{86}\text{Sr}$ versus smectite and illite contents. (c and d) ϵNd compositions versus smectite and illite contents. Red-filled circles and blue hollow circles represent cores BT-7 and CJB01-64, respectively.

Sediments from core CJB01-75 during the 7.5–0 cal ka BP period fall on the mixing curve between the Mekong River and Mae Klong River end members. The Mae Klong River end member contributes 30%–40% sediment source to core CJB01-75, which is higher than that during the 13.3–7.5 cal ka BP period of core CJB01-64 (20%–30%) (Figure 7b). Therefore, cores in the central Sunda Shelf received more sediment contributions from the Mae Klong River after 7.5 cal ka BP.

5.1.2. Clay Mineral Evidence

Clay mineralogical results obtained in this study are plotted in the ternary diagram of (illite + chlorite)-kaolinite-smectite (Figure 9), together with previous results for rivers around the Sunda Shelf (Liu et al., 2016). Clay mineral

assemblages allow us to distinguish six sedimentary provinces characterized by different compositions. These sedimentary provinces consist of the Mekong River, the rivers of northern Thailand, the rivers of southern Thailand, rivers of the east Malay Peninsula, rivers of northern Borneo, and rivers of northern Sumatra. The clay mineral assemblages from the Mekong River are dominated by illite (average 37%) and kaolinite (average 31%). The clay mineral assemblages of the rivers of northern Thailand consist predominantly of smectite (average 43%) and kaolinite (average 27%), while those of the rivers of southern Thailand are dominated by kaolinite (average 42%) and smectite (average 25%). The rivers of the Malay Peninsula display a predominance of kaolinite (average 62%). The clay mineral assemblages of Borneo's rivers consist mainly of illite (average 56%), whereas rivers of Sumatra are dominated by kaolinite (average 57%) and smectite (19%) (Figure 3b; Table S2 in Supporting Information S1).

5.1.2.1. Sediment Sources of the Gulf of Thailand: Core BT-7

For core BT-7, located in the Gulf of Thailand, clay mineral assemblages of sediments from 13.3 to 7.5 cal ka BP fall within the range for northern Thailand's rivers (Figure 9a), which are characterized by relatively high smectite contents (40%–60%). After 7.5 cal ka BP, the clay mineralogical results are also mainly plotted on the curves of northern Thailand's rivers but are characterized by lower smectite contents (25%–50%) and higher illite and chlorite contents (30%–50%), suggesting the mixing of other sources characterized by high illite and chlorite contents. In Figure 9a, clay mineral assemblages of sediments of core BT-7 fit on a mixing line between northern Thailand's rivers and the Mekong River, suggesting that higher illite and chlorite contents derive mainly from the Mekong River, which is in agreement with the Sr-Nd isotopic results (Figure 7b).

5.1.2.2. Sediment Sources of the Central Sunda Shelf: Cores CJB01-64 and CJB01-75

The clay mineralogical composition of surface sediments from the central Sunda Shelf lines up on a straight line, which plots between the field of the mineralogical composition of the Mekong River and the rivers of northern Thailand (Figure 9b). This suggests that the clay mineral composition of the central Sunda Shelf results from the mixing of clay inputs from these two sedimentary sources. Clay minerals from northern Thailand's rivers could be transported to the southern Gulf of Thailand via the sea surface currents associated with the northeastern monsoon (Shi et al., 2015). Illite and chlorite of surface sediments on the central Sunda Shelf are concentrated in the northeast region (Figures 5a and 5b). Mekong River sediments dominated by illite (average 37%) can be transported to the northeastern region of the central Sunda Shelf (Liu et al., 2016). Strong northeastern monsoon in winter causes dominant southwestward surface currents, permitting the transport of a large amount of Mekong River-suspended sediment toward the southwest (Figure 1d; Xue et al., 2010, 2012). The Mekong River sediment then enters the Sunda Shelf under cyclonic circulation in the southern SCS.

The Malay Peninsula is a potential source for the central Sunda Shelf due to its proximity. Kaolinite is the major clay mineral in the Malay Peninsula's rivers. The distribution of kaolinite contents in Figure 5c indicates that sediments from the rivers of the Malay Peninsula are mainly deposited in the offshore area and contribute only very slightly to the central shelf. During the last deglaciation, sediments from the Malay Peninsula were transported directly into the southern SCS. As the sea level rose, no significant increase in kaolinite content was found in the cores from the central Sunda Shelf before 7.5 cal ka BP (Figure 6). Besides, the modern circulation system on the Sunda Shelf was formed at around 9.5 ka (Hanebuth et al., 2011); however, there is no significant change in kaolinite content in this period (Figure 6). Therefore, the sea level and monsoon had little influence on the supply of sediment from the Malay Peninsula to the central Sunda Shelf since the last deglaciation. A similar phenomenon is also observed in the Pearl River mouth on the northern shelf of the SCS and is mainly due to the rapid sedimentation of kaolinite in a marine environment (Liu et al., 2010, 2016). Although smectite may also settle in the estuary (Li et al., 2020), kaolinite generally has a larger grain size than smectite (Chamley, 1989), and thus, kaolinite is more susceptible to settling than smectite in the river mouth.

The clay mineral variations of core CJB01-64 fall into two periods: 13.3–7.5 cal ka BP and 7.5–2.6 cal ka BP. From 13.3 to 7.5 cal ka BP, the clay mineralogical compositions, characterized by high illite and chlorite contents (35%–50%) and moderate smectite contents (25%–45%), mainly fall between fields of the mineral compositions of river sediments from northern Thailand's rivers and the Mekong River (Figure 9b). During the 7.5–2.6 cal ka BP time interval, the clay mineral assemblages are mainly plotted within the mineralogical range of northern Thailand's rivers, which is characterized by higher smectite contents (45%–65%) and lower illite and chlorite contents (20%–35%) than the previous period. The kaolinite contents show no significant variations (15%–25%) between

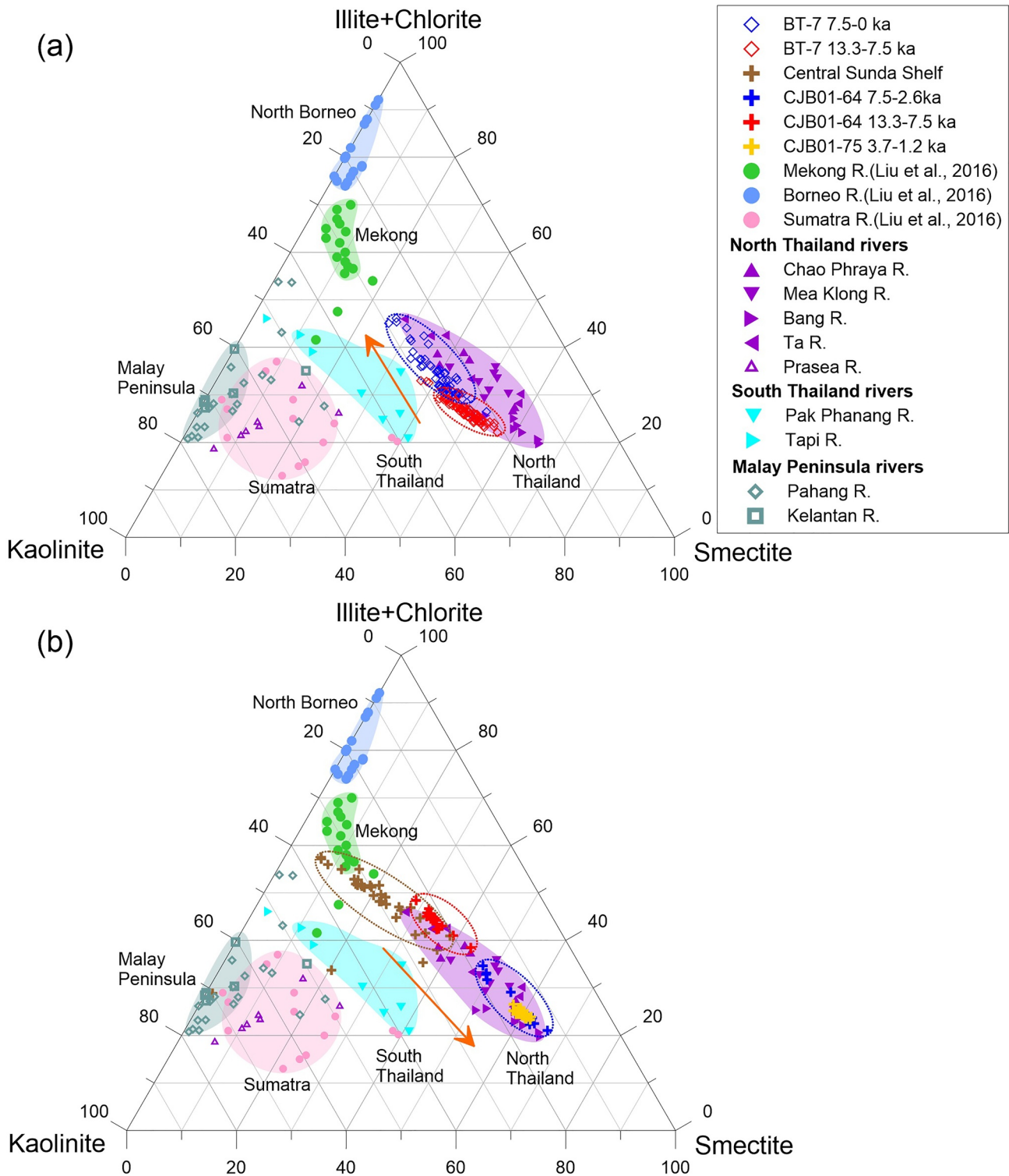


Figure 9. Ternary diagram of clay mineral groups (illite + chlorite)-kaolinite-smectite. (a) Clay mineral diagram of core BT-7 from the Gulf of Thailand. (b) Clay mineral diagram of cores CJB01-64 and CJB01-75 from the central Sunda Shelf. The orange arrows indicate the variation trends of clay mineral assemblages during the 13.3–7.5 cal ka BP and 7.5–0 cal ka BP time intervals.

these two-time intervals. The clay mineral compositions of sediments from the late Holocene (4.0–1.2 ka BP) of core CJB01-75 fall into the same range as core CJB01-64 with the same time interval, indicating that clay minerals of core CJB01-75 also derive mainly from the rivers of northern Thailand (Figure 9b). If the change in clay mineral contents in cores CJB01-75 and CJB01-64 is caused by weathering, the increase in smectite contents of these cores should be due to enhanced chemical weathering. However, the corresponding chemical weathering became weaker due to the weakened East Asian summer monsoon after 7.5 cal ka BP (Dykoski et al., 2005). Therefore, the changes in clay minerals should not be caused by changes in chemical weathering, but are more likely to be due to changes in sediment sources.

These results obtained on cores CJB01-64 and CJB01-75 suggest that before 7.5 cal ka BP, clay mineral assemblages resulted mainly from the mixing of material from northern Thailand's rivers and the Mekong River. The contribution of clay from the Mekong River to the central Sunda Shelf decreased after 7.5 cal ka BP. The detrital material from northern Thailand's rivers then becomes the dominant source of clay minerals after 7.5 cal ka BP, which is also in agreement with the Sr-Nd isotopic results (Figure 7b). The smectite content of the Mekong River did not significantly change after 13 cal ka BP (Colin et al., 2010). In particular, at 7.5 cal ka BP, no significant change in smectite content was observed in the core of Colin et al. (2010). This suggests that the Mekong River did not produce more smectite in the past or that the smectite reduced at 7.5 cal ka BP. Although Sr isotopes may be affected by weathering, no significant correlation could be observed between Sr isotopes and chemical weathering index (CIA) of sediments from rivers surrounding the Sunda Shelf ($R^2 = 8.82 \times 10^{-5}$) and core BT-7 ($R^2 = 0.34$) (Liu et al., 2016; Zhang et al., 2021), suggesting that Sr isotopic composition of the area around the Sunda Shelf is little affected by chemical weathering.

The records in the late Holocene in the cores did not present any significant variations. Changes in sediment flux due to anthropogenic impacts occurred after the dams were built in the 1990s in southeast Asia (Li et al., 2017). Therefore, the transition at 7.5 cal ka BP cannot be attributed to human activity. The major clay mineral composition (illite) of the Mekong River had a decreasing trend since the Holocene (Colin et al., 2010), whereas the chemical weathering has decreased since the Mid-Holocene, suggesting that the clay mineral composition of the Mekong River has not been affected by chemical weathering since the Holocene. Although variations of clay mineral compositions in the northern Thailand rivers through the Holocene are not available, if the drainages of the northern Thailand rivers were affected by chemical weathering, then smectite and kaolinite contents should have been higher in the early Holocene than at present. At least smectite remained the dominant clay mineral component of northern Thailand rivers during the Holocene. Indeed, smectite contents in core BT-7 were higher in the early Holocene than in the late Holocene, but kaolinite contents did not significantly change, which may be due to the different responses of smectite and kaolinite to bedrock and weathering in river drainages. However, the Sr-Nd isotopic evidence of sediment sources in the cores displays similar results with the clay minerals, which further indicates that the clay minerals are not significantly affected by chemical weathering.

5.2. East Asian Monsoon and Sea Level Control of Sediment Transport on the Sunda Shelf Since the Last Deglaciation

5.2.1. East Asian Monsoon and Sea Level Change Control Sedimentary Records

Clay mineralogical ratios and Sr-Nd isotope variations have been compared with core MD97-2150 in the southern SCS and core T93 in the Gulf of Thailand (Figure 1a) to determine the main climatic processes (monsoon and/or sea level) responsible for changes in sediment transportation patterns on the Sunda Shelf and to the southern SCS deep-basin since the last deglaciation (Figure 10). The site of core MD97-2150 was located off the mouth of the Paleo-Mekong during a glacial low sea-level stand (Liu et al., 2004). The illite content of the Mekong River sediments has decreased since the last deglaciation (Colin et al., 2010), suggesting that illite from the Mekong River was not affected by weathering during this stage. Although the exact clay mineral content during the last deglaciation was unknown, smectite remains the dominant clay mineral component of the northern Thailand rivers due to its dominant smectite content and smectite-dominated soil (Figure 3; Yoothong et al., 1997). Thus, the smectite/illite ratios of the Gulf of Thailand cores can be used to evaluate the variations of contributions between northern Thailand's rivers and the Mekong River. The smectite/illite ratios and Sr-Nd isotopes of sediments from cores BT-7, T93, CJB01-64, CJB01-75, and MD97-2150 all display obvious changes at around 7.5 cal ka BP but with different variation trends before and after 7.5 cal ka BP since the last deglaciation (Figure 10).

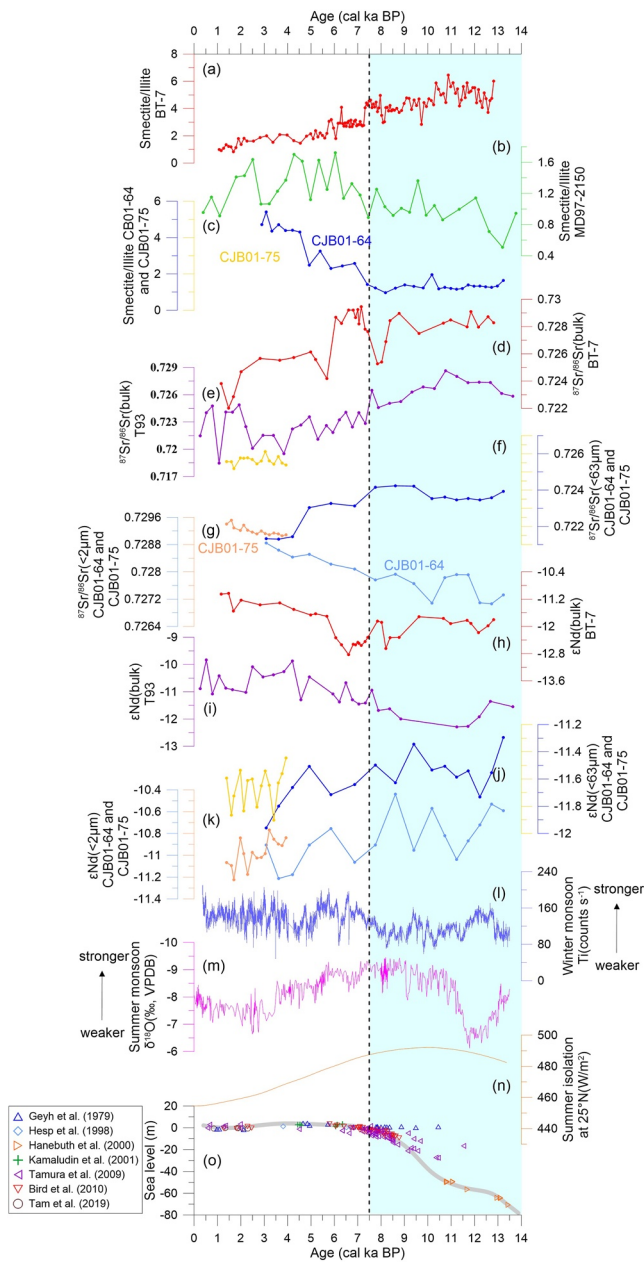


Figure 10. Comparison of the sedimentary record, climate, and sea-level changes. (a–c) Smectite/illite ratio variations of cores BT-7, MD97-2150 (Liu et al., 2004), CJB01-64, and CJB01-75. (d–k) Sr-Nd isotopic variations in cores BT-7, T93 (Chen, 2020), CJB01-64, and CJB01-75. (l and m) Winter and summer East Asian monsoon intensities (Dykoski et al., 2005; Yancheva et al., 2007). (n) Insolation received by the earth at 25°N of latitude during boreal summer (Dykoski et al., 2005). (o) Sea-level change (Bird et al., 2010; Geyh et al., 1979; Hanebuth et al., 2000; Hesp et al., 1998; Kamaludin, 2001; Tam et al., 2018; Tamura et al., 2009). The dashed line at approximately 7.5 cal ka BP indicates the boundaries of the sedimentary and climatic transitions at cores from the Sunda Shelf and southern SCS.

During the 13.3–7.5 cal ka BP time interval, relatively stable smectite/illite ratios and Sr-Nd isotopic compositions of these cores indicate stable sediment sources. The winter monsoon was weaker, whereas the summer monsoon was stronger along with strengthening summer insolation (Figures 10l–10n; Dykoski et al., 2005; Yancheva et al., 2007). The relative sea level gradually rose during this period (Figure 10o; Hanebuth et al., 2011). The clay minerals of core MD97-2150 derive from the Mekong River (Colin et al., 2010; Liu et al., 2004), while the major sediment sources of cores from the Gulf of Thailand (BT-7 and T93) are northern Thailand rivers and clay minerals of core from the central Sunda Shelf (CJB01-64) are from northern Thailand rivers and the Mekong River. Clay mineralogy and Sr-Nd isotopic compositions of cores CJB01-64, MD97-2150, and BT-7 indicate higher contributions of Mekong River sediments to the central Sunda Shelf and the southern SCS (Figures 10a–10c). The strong East Asian summer monsoon could have strengthened the southwest monsoon current and contributed to the eastward transport of Mekong River sediment into the southern SCS, although the paleovalley was gradually flooded as the sea level rose.

During the 7.5–0 cal ka BP time interval, the smectite/illite and $^{87}\text{Sr}/^{86}\text{Sr}$ ratios of cores from the Gulf of Thailand (BT-7 and T93) exhibit a decrease, while the ϵNd values display an increasing trend (Figures 10a, 10d, 10e, 10h, and 10i). On the contrary, the smectite/illite ratios of cores CJB01-64 (central Sunda Shelf) and MD97-2150 display variation trends opposite to those of core BT-7 (Gulf of Thailand). The clay mineral sources for sediments from cores BT-7, CJB01-64, and MD97-2150 over this period were therefore different from those in the 13.3–7.5 cal ka BP period. Sediments from the Gulf of Thailand (core BT-7) received a higher contribution from sediments from the Mekong River. In contrast, sediments from the central Sunda Shelf (core CJB01-64) display a lesser contribution from the Mekong River after 7.5 cal Kyr BP. Such variations in sediment sources observed in the central Sunda Shelf are also in agreement with clay mineralogical results from core MD97-2150, which also suggest a decreased contribution of illite deriving from the Mekong River (Colin et al., 2010).

The relative sea level had a last pulse rise at around 7.5 cal ka BP (Hanebuth et al., 2011) and then remained relatively stable until the present time (Figure 10o). The Mekong River delta started to form after 8–7.5 cal ka BP in conjunction with sea-level rise (Tamura et al., 2009; Tjallingii et al., 2010), while the Chao Phraya River and Mae Klong River delta similarly initiated over the last 8–7 cal ka BP, forming the central plain of Thailand (Tanabe et al., 2003). Accumulation rates were greatly reduced in the Paleo-Mekong River valley after the river-mouth system flooded and stepped back, which affected the sediment supply to deeper parts of the southeast Vietnamese shelf (Tjallingii et al., 2010). Due to rapid flooding between 9.5 and 8.5 cal ka BP, a portion of the Mekong River sediment started to deposit in the Cambodian lowlands. Meanwhile, the winter monsoon was stronger, whereas the summer monsoon was weaker along with weakening summer insolation since 9 cal ka BP (Dykoski et al., 2005; Yancheva et al., 2007). A strong winter monsoon could have been responsible for a stronger southwestward coastal current which could have efficiently transported more Mekong River sediments southwestward into the Gulf of Thailand after 7.5 cal ka BP. Additionally, the grain size of cores in the Gulf of Thailand and the central Sunda Shelf both become coarser after 7.5 cal ka BP, indicating

hydrodynamic enhancement (Figure 2). Intensifying winter monsoon increased not only physical erosion but also surface current, causing a coarser grain size after 7.5 cal ka BP. Cores from the Gulf of Thailand and the central Sunda Shelf have been flooded since the Holocene (Sathiamurthy & Voris, 2006). With the sea level rising and estuaries

retreating, the study cores received less coarse terrigenous sediment at 7.5 cal ka BP, which suggests that the coarsening grain size at 7.5 cal ka BP did not reflect the avulsion of the depositional lobes.

In addition, a morphological investigation of the Mekong River delta has shown a large down-drift of sediment and a rapid progradation over the past 3 cal ka BP around Cape Camau (Xue et al., 2010). The strong southwestward coastal current forced by the strong northeast monsoon plays an important role in the longshore transport of resuspended sediments into the Gulf of Thailand (Xue et al., 2010, 2012). Consequently, less sediment from the Mekong River was transported and deposited toward the southeastern shelf into the deeper SCS and core MD97-2150 after 7.5 cal ka BP. This is also associated with less sediment transported from the Mekong River into the central Sunda Shelf (cores CJB01-64 and CJB01-75), while more sediments from the Mekong River were transported into the Gulf of Thailand (cores BT-7 and T93).

5.2.2. Sediment Transport Model on the Sunda Shelf Since the Last Deglaciation

Based on reconstructions of the paleo-coastline since the last termination (Hanebuth et al., 2011; Sathiamurthy & Voris, 2006), we can propose a sediment transport model for the Gulf of Thailand and central Sunda Shelf since the last deglaciation. In Figure 11, the transport model is displayed for three time slices: at 12.7 cal ka BP (−60 m below modern sea level), 10.8 cal ka BP (−40 m), and 7.2 cal ka BP (−5 m).

At 12.7 cal ka BP, corresponding to the Younger Dryas event (12.87–11.9 cal ka BP; Cheng et al., 2020), the central Sunda Shelf was largely exposed. The Paleo-Mekong River sediments were directly transported into the southern SCS (core MD97-2150) through the Paleo-Mekong River valley. The Paleo-Chao Phraya River/Mae Klong River transported sediments into the central Gulf of Thailand (cores BT-7 and T93) and the central Sunda Shelf (core CJB01-64) along the paleo-Chao Phraya River valley (Figure 11a). We found that the base of the core BT-7 did not show an exposed terrestrial structure (Figure S1 in Supporting Information S1). The main components are still clay and silt and there are some stratified layers of plant debris and a lack of bioclastic debris. Therefore, it may be a swampy environment near a tributary of the Paleo-Chao Phraya River. Due to the proximity of the central Sunda Shelf (core CJB01-64) to the Indochina Peninsula over this period, the central Sunda Shelf also received detrital material from the Mekong River.

At 10.8 cal ka BP, the inner shelf region was flooded. However, the Paleo-Mekong River mouth was still close to core MD97-2150 and transported sediment into the southern SCS. A portion of the Mekong River sediments would have been transported to the central Sunda Shelf (core CJB01-64) under the southwest monsoon coastal current. The Paleo-Chao Phraya River/Mae Klong River sediments along the paleovalley were transported to the northern Gulf of Thailand and further to the middle Gulf of Thailand and the central Sunda Shelf via the coastal current (Figure 11b).

At 7.2 cal ka BP, the initiation of the Mekong River delta and coastal aggradation at the Mekong River estuary occurred in conjunction with the inundation of the Sunda Shelf. The sedimentary color difference in core BT-7 at about 7.5 cal ka BP may also indicate the flooding of the Sunda Shelf (Figure S1 in Supporting Information S1). Meanwhile, Mekong River sediments were transported to the southwest and into the Gulf of Thailand as a result of the progressive intensification of the East Asian winter monsoon. Submerging of the Paleo-Mekong/Chao Phraya valley led to a decrease in the number of Mekong River sediments transported to the margin of the southern SCS (core MD97-2150) and the central Sunda Shelf (cores CJB01-64 and CJB01-75). The reinforcement of the surface cyclonic circulation on the Sunda Shelf, due to stronger East Asian winter monsoon wind, transported sediments from the Mekong River into the Gulf of Thailand and then to the central Sunda Shelf where it mixed progressively with sediments from the rivers of northern Thailand (Figure 11c).

6. Conclusions

In this study, we have investigated grain size distribution, clay mineral assemblages, and Sr-Nd isotopic composition of sediment samples from rivers surrounding the Sunda Shelf, from the surface of the central Sunda Shelf off the Malay Peninsula, and from three gravity cores located in the central Sunda Shelf (CJB01-64 and CJB01-75) and the middle Gulf of Thailand (BT-7). Our aim has been to reconstruct the provenance of the sediments at an extremely high temporal resolution and to reveal the mechanism that triggered changes in the distribution of sediments on the paleo-Sunda Shelf since the last deglaciation. We conclude that:

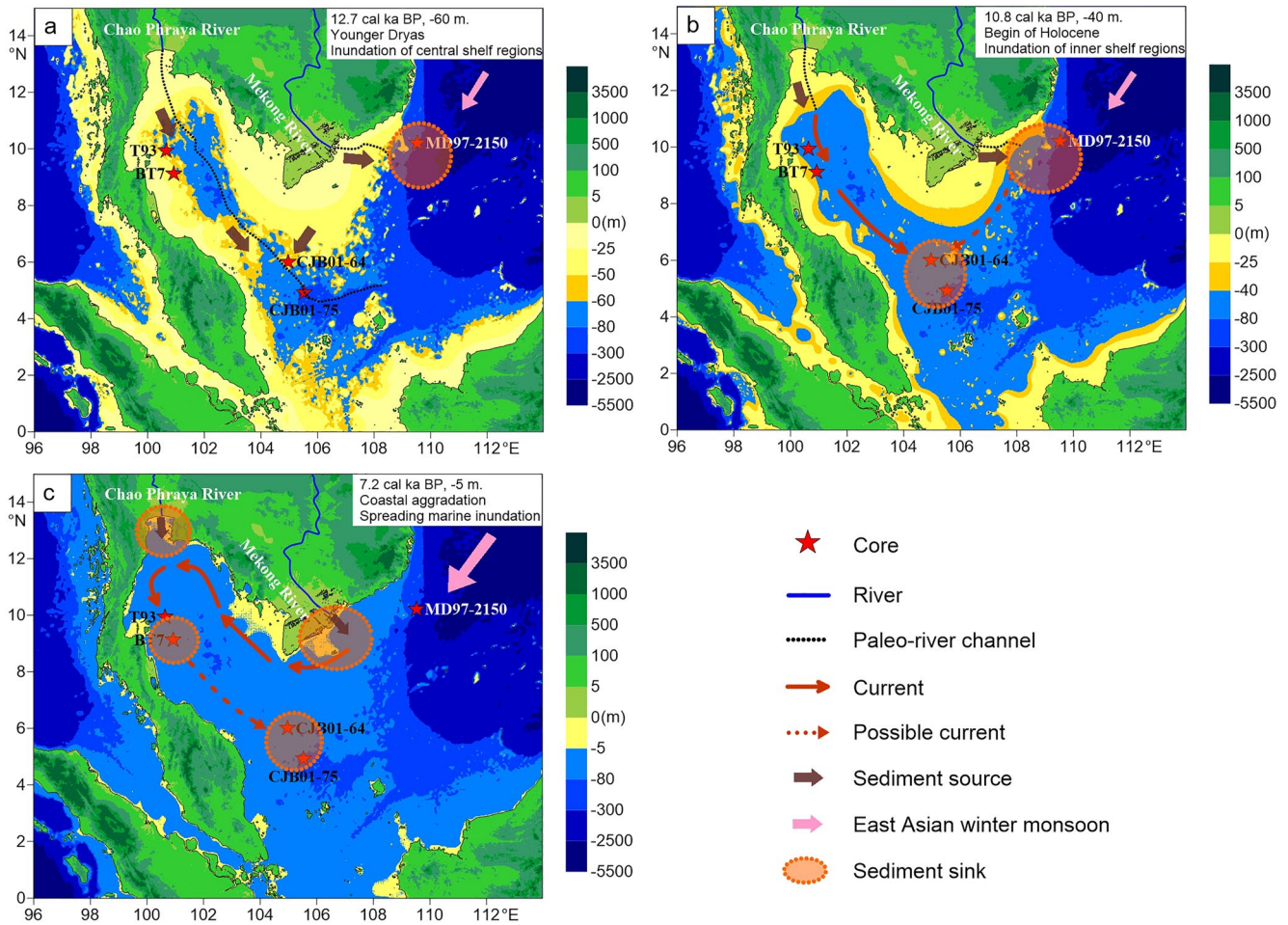


Figure 11. Transport model of sediments around the Sunda Shelf since the last deglaciation: (a) 12.7 cal ka BP (−60 m below modern sea level); (b) 10.8 cal ka BP (−40 m); (c) 7.2 cal ka BP (−5 m). Maps are adapted from Sathiamurthy and Voris (2006) and Hanebuth et al. (2011).

1. Clay mineral assemblage combined with Sr and Nd isotopic compositions allows us to discriminate sediments deriving from rivers surrounding the Sunda Shelf. The clay mineral assemblages of cores from the Sunda shelf are dominated by smectite (25%–66%) and kaolinite (21%–76%), with lesser amounts of illite (8%–31%) and chlorite (9%–21%). Sr and Nd isotopes obtained on the clay-sized fraction combined with clay mineral contents indicate that most of the smectite from the paleo-Sunda Shelf does not derive from weathering of the basaltic province of Sumatra or the Mekong River basin but derives from northern Thailand. Illite and chlorite derive mainly from the Mekong River. Kaolinite, which is a dominant mineral in rivers of the Malay Peninsula, is deposited in the offshore area and contributes only very slightly to the central Sunda Shelf. We have thus demonstrated that sediments of the central Sunda Shelf and the Gulf of Thailand result from changes in the relative contributions from the Mekong River and the rivers of northern Thailand (Chao Phraya River, Mae Klong River, Tha Chin River, and Bang Pakong River).
2. Clay mineral assemblages and Sr–Nd isotopic compositions of core BT-7 in the Gulf of Thailand and cores CJB01-64 and CJB01-75 in the central Sunda Shelf display opposite changes in sediment sources at 7.5 cal ka BP. From 13.3 to 7.5 cal ka BP, sediments of the Gulf of Thailand were derived from the rivers of northern Thailand, whereas the Gulf of Thailand received a greater contribution of sediments from the Mekong River after 7.5 cal ka BP. In contrast, sediments of the central Sunda Shelf predominantly derive from the rivers of northern Thailand and the Mekong River during the 13.3–7.5 cal ka BP period, while the central Sunda Shelf received less sediment from the Mekong River after 7.5 cal ka BP.
3. The East Asian monsoon and sea-level changes have modified sediment sources and transport on the Sunda Shelf since the last deglaciation. During the 13.3–7.5 cal ka BP time interval, the summer monsoon was strong

and controlled the discharge of Mekong River sediments toward the southeast and into the deep sea in the southern SCS. At around 7.5 cal ka BP, the rapid sea level rise resulted in major flooding of the shelf, while the East Asian winter monsoon became stronger. There was a drop in the amount of sediment transported from the Mekong River toward the southeast into the southern SCS, and more sediments from the Mekong River were gradually trapped in the estuary and transported southwesterly into the Gulf of Thailand due to a strong southwestward coastal current. Consequently, the Mekong River contributed more sediments to the Gulf of Thailand after 7.5 cal ka BP and less to the central Sunda Shelf.

Data Availability Statement

The data in this work are available at Wu (2023) with open access to download the data set. DOI: <https://data.mendeley.com/datasets/wvb2sdpwtk/1>.

Acknowledgments

We express our gratitude to the personnel of the National University of Malaysia, Phuket Marine Biological Center, Thailand, First Institute of Oceanography, Ministry of Natural Resources, China, and the crews of R.V. DISCOVERY and M.V. SEAFDEC for their contribution in collecting samples during the voyage. We extend our appreciation to Louise Bordier for her assistance in conducting Sr and Nd isotopic analyses. This research was supported by the National Program on Global Change and Air-Sea Interaction (GASI-04-HYDZ-02 and GASI-02-SCS-CJB01), the Natural Science Foundation of China-Shandong Joint Fund for Marine Science Research Centers (U1606401), the Scientific and Technological Innovation Project Financially supported by Qingdao National Laboratory for Marine Science and Technology (2015ASKJ03), the China-Malaysia cooperation project "Effect on the variability of seasonal monsoon on the sedimentary process in Peninsular Malaysia waters," China-Thailand cooperation project "Research on Vulnerability of Coastal Zones," the Basic Scientific Fund for National Public Research Institutes of China (GY0223Q03), and the Taishan Scholar Program of Shandong (tspd20181216).

References

- Alqahtani, F. A., Johnson, H. D., Jackson, C. A. L., & Som, M. R. B. (2015). Nature, origin and evolution of a Late Pleistocene incised valley-fill, Sunda Shelf, Southeast Asia. *Sedimentology*, 62(4), 1198–1232. <https://doi.org/10.1111/sed.12185>
- Armstrong, E., Hopcroft, P. O., & Valdes, P. J. (2019). A simulated Northern Hemisphere terrestrial climate dataset for the past 60,000 years. *Scientific Data*, 6(1), 265. <https://doi.org/10.1038/s41597-019-0277-1>
- Bayon, G., Toucanne, S., Skonieczny, C., André, L., Bermell, S., Cheron, S., et al. (2015). Rare earth elements and neodymium isotopes in world river sediments revisited. *Geochimica et Cosmochimica Acta*, 170, 17–38. <https://doi.org/10.1016/j.gca.2015.08.001>
- Bird, M., Austin, W., Wurster, C., Fifield, L., Mojtahid, M., & Sargeant, C. (2010). Punctuated eustatic sea-level rise in the early mid-Holocene. *Geology*, 38(9), 803–806. <https://doi.org/10.1130/g31066.1>
- Blaauw, M., & Christen, J. A. (2011). Flexible paleoclimate age-depth models using an autoregressive gamma process. *Bayesian Analysis*, 6(3), 457–474. <https://doi.org/10.1214/11-ba618>
- Blum, J. D., & Erel, Y. (1995). A silicate weathering mechanism linking increase in marine $^{87}\text{Sr}/^{86}\text{Sr}$ with global glaciation. *Nature*, 373(6513), 415–418. <https://doi.org/10.1038/373415a0>
- Boulay, S., Colin, C., Trentesaux, A., Clain, S., Liu, Z., & Lauer-Leredde, C. (2007). Sedimentary responses to the Pleistocene climatic variations recorded in the South China Sea. *Quaternary Research*, 68(1), 162–172. <https://doi.org/10.1016/j.yqres.2007.03.004>
- Boulay, S., Colin, C., Trentesaux, A., Frank, N., & Liu, Z. (2005). Sediment sources and East Asian monsoon intensity over the last 450 ky. Mineralogical and geochemical investigations on the South China Sea sediments. *Palaeogeography, Palaeoclimatology, Palaeoecology*, 228(3–4), 260–277. <https://doi.org/10.1016/j.palaeo.2005.06.005>
- Carter, S., Griffith, E., Clift, P., Scher, H., & Dellapenna, T. (2020). Clay-fraction strontium and neodymium isotopes in the Indus Fan: Implications for sediment transport and provenance. *Geological Magazine*, 157(6), 879–894. <https://doi.org/10.1017/s0016756820000394>
- Chamley, H. (1989). *Clay sedimentology* (p. 623). Springer.
- Chen, Y. (2020). Sediment provenance evolution in the Gulf of Thailand since the last deglacial: Evidence from elements and Sr, Nd isotopes. Master Thesis. Nanjing University.
- Cheng, H., Zhang, H., Spötl, C., Sinha, A., Li, H., Bartolomé, M., et al. (2020). Timing and structure of the Younger Dryas event and its underlying climate dynamics. *Proceedings of the National Academy of Sciences of the United States of America*, 117(38), 23408–23417. <https://doi.org/10.1073/pnas.2007869117>
- Chu, P. C., & Wang, G. (2003). Seasonal variability of thermohaline front in the central South China Sea. *Journal of Oceanography*, 59(1), 65–78. <https://doi.org/10.1023/a:1022868407012>
- Clift, P. D. (2016). Assessing effective provenance methods for fluvial sediment in the South China Sea. *Geological Society, London, Special Publications*, 429(1), 9–29. <https://doi.org/10.1144/sp429.3>
- Colin, C., Siani, G., Sicre, M.-A., & Liu, Z. (2010). Impact of the East Asian monsoon rainfall changes on the erosion of the Mekong River basin over the past 25 000 yr. *Marine Geology*, 271(1–2), 84–92. <https://doi.org/10.1016/j.margeo.2010.01.013>
- Colin, C., Turpin, L., Bertaux, J., Desprairies, A., & Kissel, C. (1999). Erosional history of the Himalayan and Burman ranges during the last two glacial-interglacial cycles. *Earth and Planetary Science Letters*, 171(4), 647–660. [https://doi.org/10.1016/s0012-821x\(99\)00184-3](https://doi.org/10.1016/s0012-821x(99)00184-3)
- Colin, C., Turpin, L., Blamart, D., Frank, N., Kissel, C., & Duchamp, S. (2006). Evolution of weathering patterns in the Indo-Burman Ranges over the last 280 Kyr: Effects of sediment provenance on $^{87}\text{Sr}/^{86}\text{Sr}$ ratios tracer. *Geochemistry, Geophysics, Geosystems*, 7(3), Q03007. <https://doi.org/10.1029/2005gc000962>
- Copard, K., Colin, C., Douville, E., Freiwald, A., Gudmundsson, G., De Mol, B., & Frank, N. (2010). Nd isotopes in deep-sea corals in the North-eastern Atlantic. *Quaternary Science Reviews*, 29(19–20), 2499–2508. <https://doi.org/10.1016/j.quascirev.2010.05.025>
- Deng, J., Wang, C., Zi, J. W., Xia, R., & Li, Q. (2018). Constraining subduction-collision processes of the Paleo-Tethys along the Changning-Menglian Suture: New zircon U-Pb ages and Sr-Nd-Pb-Hf-O isotopes of the Lincang Batholith. *Gondwana Research*, 62, 75–92. <https://doi.org/10.1016/j.gr.2017.10.008>
- Desiège, P. A., St-Onge, G., Duchesne, M. J., Montero-Serrano, J. C., & Haller, M. J. (2023). Late Pleistocene and Holocene transgression inferred from the sediments of the Gulf of San Jorge, central Patagonia, Argentina. *Journal of Quaternary Science*, 38(5), 629–646. <https://doi.org/10.1002/jqs.3511>
- Dykoski, C., Edwards, R., Cheng, H., Yuan, D., Cai, Y., Zhang, M., et al. (2005). A high-resolution, absolute-dated Holocene and deglacial Asian monsoon record from Dongge Cave, China. *Earth and Planetary Science Letters*, 233(1–2), 71–86. <https://doi.org/10.1016/j.epsl.2005.01.036>
- Fang, G., Fang, W., Fang, Y., & Wang, K. (1998). A survey of studies on the South China Sea upper ocean circulation. *Acta Oceanographica Taiwan*, 37, 1–6.
- Geyh, M., Streif, H., & Kudrass, H. (1979). Sea-level changes during the late Pleistocene and Holocene in the Strait of Malacca. *Nature*, 278(5703), 441–443. <https://doi.org/10.1038/278441a0>
- Hanebuth, T., Statterger, K., & Bojanowski, A. (2009). Termination of the Last Glacial Maximum sea-level lowstand: The Sunda-Shelf data revisited. *Global and Planetary Change*, 66(1–2), 76–84. <https://doi.org/10.1016/j.gloplacha.2008.03.011>

- Hanebuth, T., Stattegger, K., & Grootes, P. (2000). Rapid flooding of the Sunda Shelf: A late-glacial sea-level record. *Science*, 288(5468), 1033–1035. <https://doi.org/10.1126/science.288.5468.1033>
- Hanebuth, T., Stattegger, K., Schimanski, A., Lüdmann, T., & Wong, H. (2003). Late Pleistocene forced-regressive deposits on the Sunda Shelf (Southeast Asia). *Marine Geology*, 199(1–2), 139–157. [https://doi.org/10.1016/s0025-3227\(03\)00129-4](https://doi.org/10.1016/s0025-3227(03)00129-4)
- Hanebuth, T., Voris, H., Yokoyama, Y., Saito, Y., & Okuno, J. (2011). Formation and fate of sedimentary depocentres on Southeast Asia's Sunda Shelf over the past sea-level cycle and biogeographic implications. *Earth-Science Reviews*, 104(1–3), 92–110. <https://doi.org/10.1016/j.earscirev.2010.09.006>
- Heaton, T. J., Köhler, P., Butzin, M., Bard, E., Reimer, R. W., Austin, W. E., et al. (2020). Marine20—the marine radiocarbon age calibration curve (0–55,000 cal BP). *Radiocarbon*, 62(4), 779–820. <https://doi.org/10.1017/rdc.2020.68>
- Hesp, P., Hung, C., Hilton, M., Ming, C., & Turner, I. (1998). A first tentative Holocene sea-level curve for Singapore. *Journal of Coastal Research*, 308–314.
- Hu, D., Böning, P., Köhler, C. M., Hillier, S., Pressling, N., Wan, S., et al. (2012). Deep sea records of the continental weathering and erosion response to East Asian monsoon intensification since 14 ka in the South China Sea. *Chemical Geology*, 326, 1–18. <https://doi.org/10.1016/j.chemgeo.2012.07.024>
- Jacobsen, S., & Wasserburg, G. (1980). Sm-Nd isotopic evolution of chondrites. *Earth and Planetary Science Letters*, 50(1), 139–155. [https://doi.org/10.1016/0012-821x\(80\)90125-9](https://doi.org/10.1016/0012-821x(80)90125-9)
- Jiang, H., Li, W. Q., Jiang, S. Y., Wang, H., & Wei, X. P. (2017). Geochronological, geochemical and Sr-Nd-Hf isotopic constraints on the petrogenesis of Late Cretaceous A-type granites from the Sibumasu Block, Southern Myanmar, SE Asia. *Lithos*, 268, 32–47. <https://doi.org/10.1016/j.lithos.2016.11.005>
- Jiwarungrueangkul, T., Liu, Z., Stattegger, K., & Sang, P. N. (2019). Reconstructing chemical weathering intensity in the Mekong River basin since the Last Glacial Maximum. *Paleoceanography and Paleoclimatology*, 34(11), 1710–1725. <https://doi.org/10.1029/2019pa003608>
- Jiwarungrueangkul, T., Liu, Z., & Zhao, Y. (2019). Terrigenous sediment input responding to sea level change and East Asian monsoon evolution since the last deglaciation in the southern South China Sea. *Global and Planetary Change*, 174, 127–137. <https://doi.org/10.1016/j.gloplacha.2019.01.011>
- Jonell, T., Li, Y., Blusztajn, J., Giosan, L., & Clift, P. (2018). Signal or noise? Isolating grain size effects on Nd and Sr isotope variability in Indus delta sediment provenance. *Chemical Geology*, 485, 56–73. <https://doi.org/10.1016/j.chemgeo.2018.03.036>
- Kamaludin, B. H. (2001). Holocene sea level changes in Kelang and Kuantan, Peninsula Malaysia. PhD thesis. University of Durham.
- Lan, C. Y., Chung, S. L., Van Long, T., Lo, C. H., Lee, T. Y., Mertzman, S. A., & Jiun-San Shen, J. (2003). Geochemical and Sr-Nd isotopic constraints from the Kontum massif, central Vietnam on the crustal evolution of the Indochina block. *Precambrian Research*, 122(1–4), 7–27. [https://doi.org/10.1016/s0301-9268\(02\)00205-x](https://doi.org/10.1016/s0301-9268(02)00205-x)
- Li, X., Liu, J. P., Saito, Y., & Nguyen, V. L. (2017). Recent evolution of the Mekong Delta and the impacts of dams. *Earth-Science Reviews*, 175, 1–17. <https://doi.org/10.1016/j.earscirev.2017.10.008>
- Li, Y., Clift, P. D., Murray, R. W., Exnicios, E., Ireland, T., & Böning, P. (2020). Asian summer monsoon influence on chemical weathering and sediment provenance determined by clay mineral analysis from the Indus Submarine Canyon. *Quaternary Research*, 93, 23–39. <https://doi.org/10.1017/qua.2019.44>
- Liu, Z., Colin, C., Huang, W., Le, K., Tong, S., Chen, Z., & Trentesaux, A. (2007). Climatic and tectonic controls on weathering in South China and the Indochina Peninsula: Clay mineralogical and geochemical investigations from the Pearl, Red, and Mekong drainage basins. *Geochemistry, Geophysics, Geosystems*, 8(5), Q05005. <https://doi.org/10.1029/2006gc001490>
- Liu, Z., Colin, C., Li, X., Zhao, Y., Tuo, S., Chen, Z., et al. (2010). Clay mineral distribution in surface sediments of the northeastern South China Sea and surrounding fluvial drainage basins: Source and transport. *Marine Geology*, 277(1–4), 48–60. <https://doi.org/10.1016/j.margeo.2010.08.010>
- Liu, Z., Colin, C., Trentesaux, A., Blamart, D., Bassinot, F., Siani, G., & Sicre, M. (2004). Erosional history of the eastern Tibetan Plateau over past 190 Kyr: Clay mineralogical investigations from the southwestern South China Sea. *Marine Geology*, 209(1–4), 1–18. <https://doi.org/10.1016/j.margeo.2004.06.004>
- Liu, Z., Colin, C., Trentesaux, A., Siani, G., Frank, N., Blamart, D., & Segueni, F. (2005). Late quaternary climatic control on erosion and weathering in the eastern Tibetan Plateau and the Mekong Basin. *Quaternary Research*, 63(3), 316–328. <https://doi.org/10.1016/j.yqres.2005.02.005>
- Liu, Z., Wang, H., Hantoro, W. S., Sathiamurthy, E., Colin, C., Zhao, Y., & Li, J. (2012). Climatic and tectonic controls on chemical weathering in tropical Southeast Asia (Malay Peninsula, Borneo, and Sumatra). *Chemical Geology*, 291, 1–12. <https://doi.org/10.1016/j.chemgeo.2011.11.015>
- Liu, Z., Zhao, Y., Colin, C., Siringan, F. P., & Wu, Q. (2009). Chemical weathering in Luzon, Philippines from clay mineralogy and major-element geochemistry of river sediments. *Applied Geochemistry*, 24(11), 2195–2205. <https://doi.org/10.1016/j.apgeochem.2009.09.025>
- Liu, Z., Zhao, Y., Colin, C., Stattegger, K., Wiesner, M., Huh, C., et al. (2016). Source-to-sink transport processes of fluvial sediments in the South China Sea. *Earth-Science Reviews*, 153, 238–273. <https://doi.org/10.1016/j.earscirev.2015.08.005>
- Lugmair, G., Shimamura, T., Lewis, R., & Anders, E. (1983). Samarium-146 in the early solar system: Evidence from neodymium in the Allende meteorite. *Science*, 222(4627), 1015–1018. <https://doi.org/10.1126/science.222.4627.1015>
- Metcalfe, I. (2013). Tectonic evolution of the Malay Peninsula. *Journal of Asian Earth Sciences*, 76, 195–213. <https://doi.org/10.1016/j.jseas.2012.12.011>
- Milliman, J., & Farnsworth, K. (2011). *River discharge to the coastal ocean: A global synthesis*. Cambridge University Press.
- Milliman, J., Farnsworth, K., & Albertin, C. (1999). Flux and fate of fluvial sediments leaving large islands in the East Indies. *Journal of Sea Research*, 41(1–2), 97–107. [https://doi.org/10.1016/s1385-1101\(98\)00040-9](https://doi.org/10.1016/s1385-1101(98)00040-9)
- Milliman, J., & Syvitski, J. (1992). Geomorphic/tectonic control of sediment discharge to the ocean: The importance of small mountainous rivers. *The Journal of Geology*, 100(5), 525–544. <https://doi.org/10.1086/629606>
- Qiao, S., Shi, X., Fang, X., Liu, S., Kornkanitnan, N., Gao, J., et al. (2015). Heavy metal and clay mineral analyses in the sediments of Upper Gulf of Thailand and their implications on sedimentary provenance and dispersion pattern. *Journal of Asian Earth Sciences*, 114, 488–496. <https://doi.org/10.1016/j.jseas.2015.04.043>
- Sang, P. N., Liu, Z., & Colin, C. (2022). Chemical weathering of the Mekong River basin with implication for East Asian monsoon evolution during the late Quaternary: Marine sediment records in the southern South China Sea. *Frontiers in Earth Science*, 1027. <https://doi.org/10.3389/feart.2022.885547>
- Sathiamurthy, E., & Voris, H. (2006). Maps of Holocene sea level transgression and submerged lakes on the Sunda Shelf. *Tropical Natural History*, 2, 1–44.
- Shi, X., Liu, S., Fang, X., Qiao, S., Khokiattiwong, S., & Kornkanitnan, N. (2015). Distribution of clay minerals in surface sediments of the western Gulf of Thailand: Sources and transport patterns. *Journal of Asian Earth Sciences*, 105, 390–398. <https://doi.org/10.1016/j.jseas.2015.02.005>

- Southon, J., Kashgarian, M., Fontugne, M., Metivier, B., & Yim, W. (2002). Marine reservoir corrections for the Indian Ocean and Southeast Asia. *Radiocarbon*, 44(1), 167–180. <https://doi.org/10.1017/s0033822200064778>
- Staub, J., & Gastaldo, R. (2000). Seasonal sediment transport and deposition in the Rajang River delta, Sarawak, East Malaysia. *Sedimentary Geology*, 133(3–4), 249–264. [https://doi.org/10.1016/s0037-0738\(00\)00042-7](https://doi.org/10.1016/s0037-0738(00)00042-7)
- Stuiver, M., & Polach, H. (1977). Discussion reporting of ¹⁴C data. *Radiocarbon*, 19(3), 355–363. <https://doi.org/10.1017/s0033822200003672>
- Tam, C., Zong, Y., Hassan, K., Ismal, H., Jamil, H., Xiong, H., et al. (2018). A below-the-present late Holocene relative sea level and the glacial isostatic adjustment during the Holocene in the Malay Peninsula. *Quaternary Science Reviews*, 201, 206–222. <https://doi.org/10.1016/j.quascirev.2018.10.009>
- Tamura, T., Saito, Y., Sieng, S., Ben, B., Kong, M., Sim, I., et al. (2009). Initiation of the Mekong River delta at 8 ka: Evidence from the sedimentary succession in the Cambodian lowland. *Quaternary Science Reviews*, 28(3–4), 327–344. <https://doi.org/10.1016/j.quascirev.2008.10.010>
- Tanabe, S., Saito, Y., Sato, Y., Suzuki, Y., Sinsakul, S., Tiyaipairach, S., & Chaimanee, N. (2003). Stratigraphy and Holocene evolution of the mud-dominated Chao Phraya delta, Thailand. *Quaternary Science Reviews*, 22(8–9), 789–807. [https://doi.org/10.1016/s0277-3791\(02\)00242-1](https://doi.org/10.1016/s0277-3791(02)00242-1)
- Tanaka, T., Togashi, S., Kamioka, H., Amakawa, H., Kagami, H., Hamamoto, T., et al. (2000). JNd-1: A neodymium isotopic reference in consistency with LaJolla neodymium. *Chemical Geology*, 168(3–4), 279–281. [https://doi.org/10.1016/s0009-2541\(00\)00198-4](https://doi.org/10.1016/s0009-2541(00)00198-4)
- Tangang, F., Xia, C., Qiao, F., Juneng, L., & Shan, F. (2011). Seasonal circulations in the Malay Peninsula Eastern continental shelf from a wave-tide-circulation coupled model. *Ocean Dynamics*, 61(9), 1317–1328. <https://doi.org/10.1007/s10236-011-0432-5>
- Tjallingii, R., Statterger, K., Wetzel, A., & Van Phach, P. (2010). Infilling and flooding of the Mekong River incised valley during deglacial sea-level rise. *Quaternary Science Reviews*, 29(11–12), 1432–1444. <https://doi.org/10.1016/j.quascirev.2010.02.022>
- Wan, S., Clift, P. D., Zhao, D., Hovius, N., Munhoven, G., France-Lanord, C., et al. (2017). Enhanced silicate weathering of tropical shelf sediments exposed during glacial lowstands: A sink for atmospheric CO₂. *Geochimica et Cosmochimica Acta*, 200, 123–144. <https://doi.org/10.1016/j.gca.2016.12.010>
- Wan, S., Toucanne, S., Clift, P. D., Zhao, D., Bayon, G., Yu, Z., et al. (2015). Human impact overwhelms long-term climate control of weathering and erosion in southwest China. *Geology*, 43(5), 439–442. <https://doi.org/10.1130/g36570.1>
- Wang, B., Huang, F., Wu, Z., Yang, J., Fu, X., & Kikuchi, K. (2009). Multi-scale climate variability of the South China Sea monsoon: A review. *Dynamics of Atmospheres and Oceans*, 47(1–3), 15–37. <https://doi.org/10.1016/j.dynatmoce.2008.09.004>
- Wattayakorn, G., King, B., Wolanski, E., & Suthanaruk, P. (1998). Seasonal dispersion of petroleum contaminants in the Gulf of Thailand. *Continental Shelf Research*, 18(6), 641–659. [https://doi.org/10.1016/s0278-4343\(97\)00072-1](https://doi.org/10.1016/s0278-4343(97)00072-1)
- Wei, G., Liu, Y., Ma, J., Xie, L., Chen, J., Deng, W., & Tang, S. (2012). Nd, Sr isotopes and elemental geochemistry of surface sediments from the South China Sea: Implications for provenance tracing. *Marine Geology*, 319, 21–34. <https://doi.org/10.1016/j.margeo.2012.05.007>
- Wu, K. (2023). Data of the river sediment, surface sediment, and sediment cores of the Sunda Shelf [Dataset]. Mendeley Data, V1. <https://doi.org/10.17632/wvb2sdpwtk.1>
- Wu, K., Liu, S., Kandasamy, S., Jin, A., Lou, Z., Li, J., et al. (2019). Grain-size effect on rare earth elements in Pahang River and Kelantan River, Peninsular Malaysia: Implications for sediment provenance in the southern South China Sea. *Continental Shelf Research*, 189, 103977. <https://doi.org/10.1016/j.csr.2019.103977>
- Wu, K., Liu, S., Shi, X., Colin, C., Bassinot, F., Lou, Z., et al. (2022). Size distribution effect on the geochemistry and mineralogy of tropical river sediments and its implications regarding chemical weathering and fractionation of alkali elements. *Lithosphere*, 8425818.
- Wu, K., Shi, X., Lou, Z., Wu, B., Li, J., Zhang, H., et al. (2021). Sedimentary responses to climate changes and human activities over the past 7400 years in the western Sunda Shelf. *Frontiers in Earth Science*, 9, 631815. <https://doi.org/10.3389/feart.2021.631815>
- Xue, Z., He, R., Liu, J., & Warner, J. C. (2012). Modeling transport and deposition of the Mekong River sediment. *Continental Shelf Research*, 37, 66–78. <https://doi.org/10.1016/j.csr.2012.02.010>
- Xue, Z., Liu, J., DeMaster, D., Van Nguyen, L., & Ta, T. (2010). Late Holocene evolution of the Mekong subaqueous delta, southern Vietnam. *Marine Geology*, 269(1–2), 46–60. <https://doi.org/10.1016/j.margeo.2009.12.005>
- Yancheva, G., Nowaczyk, N., Mingram, J., Dulski, P., Schettler, G., Negendank, J., et al. (2007). Influence of the intertropical convergence zone on the East Asian monsoon. *Nature*, 445(7123), 74–77. <https://doi.org/10.1038/nature05431>
- Yoothong, K., Moncharoen, L., Vijarnson, P., & Eswaran, H. (1997). Clay mineralogy of Thai soils. *Applied Clay Science*, 11(5–6), 357–371. [https://doi.org/10.1016/s0169-1317\(96\)00033-6](https://doi.org/10.1016/s0169-1317(96)00033-6)
- Zhang, H., Hu, P., Cao, L., Tampubolon, A., Liu, A., Cheng, X., et al. (2020). Geochemical characteristics and Sr-Nd-Hf isotope compositions of Late Triassic post-collisional A-type granites in Sarudik, SW Sumatra, Indonesia. *Island Arc*, 29(1), e12357. <https://doi.org/10.1111/iar.12357>
- Zhang, H., Liu, S., Wu, K., Cao, P., Pan, H. J., Wang, H., et al. (2021). Evolution of sedimentary environment in the Gulf of Thailand since the last deglaciation. *Quaternary International*, 629, 36–43. <https://doi.org/10.1016/j.quaint.2021.02.018>